



Towards Ensemble-Based Kilometer-Scale Climate Simulations over the Third Pole Region

Andreas F. Prein¹ · Nikolina Ban² · Tinghai Ou⁷ · Jianping Tang¹¹ · Koichi Sakaguchi³ · Emily Collier² · Sanjay Jayanarayanan⁴ · Lu Li⁵ · Stefan Sobolowski⁵ · Xingchao Chen⁶ · Xu Zhou⁸ · Hui-Wen Lai⁷ · Shiori Sugimoto⁹ · Liwei Zou¹² · Shabeh ul Hasson¹³ · Marie Ekstrom¹⁴ · Praveen Kumar Pothapakula^{16,17} · Bodo Ahrens¹⁶ · Romilly Stuart^{15,18} · Hans Christian Steen-Larsen¹⁵ · Ruby Leung³ · Danijel Belusic^{10,19} · Julia Kukulies⁷ · Julia Curio⁷ · Deliang Chen⁷

Received: 20 April 2022 / Accepted: 12 October 2022

© The Author(s), under exclusive licence to Springer-Verlag GmbH Germany, part of Springer Nature 2022

Abstract

The Tibetan Plateau and its surrounding mountains have an average elevation of 4,400 m and a glaciated area of ~100,000 km² giving it the name “Third Pole (TP) region”. The TP is the headwater of many major rivers in Asia that provide fresh water to hundreds of millions of people. Climate change is altering the energy and water cycle of the TP at a record pace but the future of this region is highly uncertain due to major challenges in simulating weather and climate processes in this complex area. The Convection-Permitting Third Pole (CPTP) project is a Coordinated Regional Downscaling Experiment (CORDEX) Flagship Pilot Study (FPS) that aims to revolutionize our understanding of climate change impacts on the TP through ensemble-based, kilometer-scale climate modeling. Here we present the experimental design and first results from multi-model, multi-physics ensemble simulations of three case studies. The five participating modeling systems show high performance across a range of meteorological situations and are close to having “observational quality” in simulating precipitation and near-surface temperature. This is partly due to the large differences between observational datasets in this region, which are the leading source of uncertainty in model evaluations. However, a systematic cold bias above 2000 m exists in most modeling systems. Model physics sensitivity tests performed with the Weather Research and Forecasting (WRF) model show that planetary boundary layer (PBL) physics and microphysics contribute equally to model uncertainties. Additionally, larger domains result in better model performance. We conclude by describing high-priority research needs and the next steps in the CPTP project.

Keywords Kilometer-scale modeling · Third Pole Region · CORDEX · Ensembles

1 Introduction

One of the largest stores of ice and snow, outside of the Arctic and Antarctic is the Tibetan Plateau and surrounding mountain ranges, known as the Third Pole (TP) Yao et al. (2012). The TP plays a significant role in the atmospheric circulation of the Northern Hemisphere Plumb (1985) and the global climate system more generally, and is highly sensitive to human-induced climate change Pörtner et al. (2019). Additionally, the TP is the headwater region of many major Asian rivers including the Indus, Brahmaputra, Ganges, Mekong, Yellow, and the Yangtze providing freshwater to hundreds of millions of people Zhang et al. (2019). Because of the TP’s complex terrain and harsh environment, ground-based observations are scarce and satellite observations are

Andreas F. Prein, Nikolina Ban, Tinghai Ou, Jianping Tangy, Koichi Sakaguchi, Emily Collier, Sanjay Jayanarayanan, Lu Li, Stefan Sobolowski, Xingchao Chen, Xu Zhou, Hui-Wen Lai, Shiori Sugimoto, Liwei Zou, Shabeh ul Hasson, Marie Ekstrom, Bodo Ahrens, Romilly Stuart, Hans Christian Steen-Larsen, Ruby Leung, Danijel Belusic, Julia Kukulies, Julia Curio and Deliang Chen contributed equally to this work.

✉ Andreas F. Prein
prein@ucar.edu

Extended author information available on the last page of the article

error-prone Tang et al. (2020), which hampers efforts to study regionally important physical processes, systems, and the effect of climate change on the TP water cycle. Horizontal resolutions of prevailing global reanalysis datasets are generally coarser than 30 km. This is not sufficient to accurately reproduce precipitation over steep topography or arising from convection and other mesoscale systems that are characterized by small-scale variability (see e.g., Maussion et al. 2014). As a result, our understanding of the impacts of climate change on the TP and downstream regions remains incomplete.

One of the main visions of CORDEX (Coordinated Regional Climate Downscaling Experiment) is to advance and coordinate science and application of regional climate downscaling through global collaborations Giorgi and Gutowski (2015). These regional climate downscaling techniques are used to provide higher-resolution climate information at regional and local scales that conventional global climate models (GCMs) cannot represent. Standard dynamical downscaling in CORDEX experiments is done at the grid spacing of 12–50 km, and they do indeed add value at regional scales in comparison to GCMs (see e.g., Torma et al. 2015). However, decreasing the grid spacing of regional climate models (RCMs) from 50 km to 12 km does not always show a clear benefit (Kotlarski et al. 2014; Prein et al. 2016; Hasson et al. 2016).

To solve emerging scientific challenges¹ that cannot be addressed within the general CORDEX framework, a more targeted experimental setup, so-called “Flagship Pilot Studies (FPS)” were initiated. These are intended to enable the CORDEX community to better address a number of the challenges in a coordinated way Gutowski et al. (2016). One such challenge is to better understand regional and local processes and phenomena relevant to climate change that cannot be investigated with standard CORDEX simulations and for which even higher-resolution simulations are needed Hasson et al. (2019). Such phenomena include extreme precipitation producing storms such as mesoscale convective systems (MCSs) Clark et al. (2016); Prein et al. (2021), orographic precipitation Rasmussen et al. (2011), snowpack dynamics Rasmussen et al. (2014), or land-atmosphere coupling Barlage et al. (2021).

Over recent years, climate simulations with a grid spacing around 5 km and less are emerging over different regions of the world and underline the importance of explicit treatment of convection in climate models Prein et al. (2015). Such kilometer-scale models typically do not use deep convection parametrizations, which are large sources of uncertainty in climate simulations Mooney et al. (2017). An increase in

the resolution and explicit treatment of convection has led to major improvements in the simulation of precipitation (Kendon et al. 2012; Prein et al. 2013; Ban et al. 2014; Prein et al. 2015), clouds (Hentgen et al. 2019), snow cover (Ikeda et al. 2010; Rasmussen et al. 2011, 2014; Liu et al. 2017; Lüthi et al. 2019), and local wind systems like sea-breezes (Belušić et al. 2018). In addition to better performance, such simulations also show differences in the climate change signal when compared to coarser-resolution models (Kendon et al. 2014; Ban et al. 2015; Kendon et al. 2019; Prein et al. 2021).

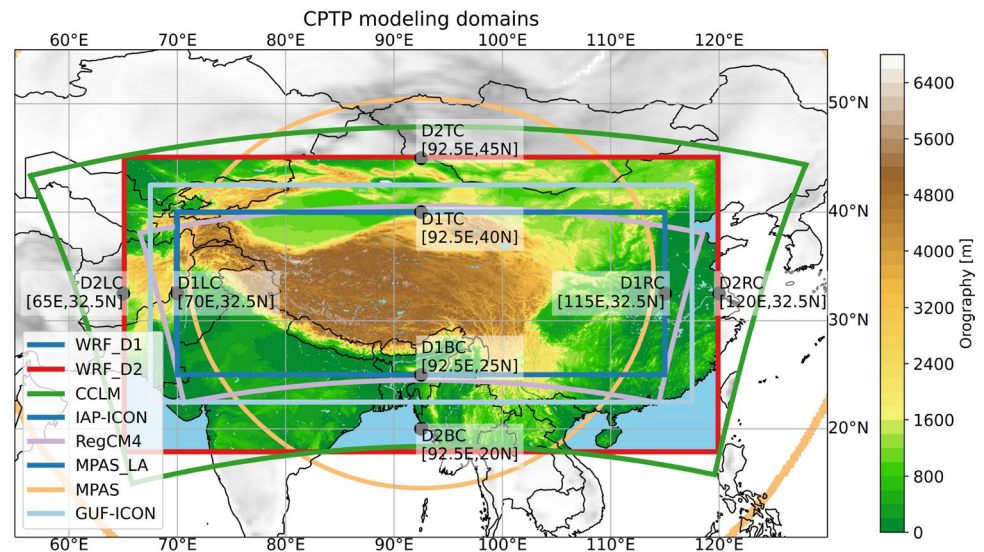
Recent studies employing kilometer-scale models over the TP region have shown its potential in resolving local processes in complex terrain such as valley winds and their interactions with large-scale forcing. Resolving such processes at a kilometer or sub-kilometer scale realistically reproduces the diurnal and seasonal cycle characteristics, lapse rate, the spatial distribution of climatic variables, precipitation frequency and intensity, and water vapor transport towards the TP Karki et al. (2017); Lin et al. (2018); Li et al. (2021); Karki et al. (2020); Sugimoto et al. (2021).

Until recently, convection-permitting studies were typically performed with only one model and for one region. However, in the last years, multi-model high-resolution, ensemble simulations started to emerge. For instance, Kendon et al. (2019) presented a twelve-member ensemble of km-scale projections (spanning three 20-year periods) providing an initial estimate of uncertainties at km-scales and sampling the uncertainty in the model physics of the driving model but not in the km-scale model itself. One of the first multi-model km-scale was produced within the CORDEX FPS on Convective Phenomena over Europe and the Mediterranean (Coppola et al. 2020). Ban et al. (2021) presented a set of 23 simulations conducted with 6 different regional climate models over the greater Alpine region. The results are encouraging, as they confirm previous findings of a large reduction of biases in precipitation diurnal cycle and heavy precipitation. Furthermore, they indicate that the uncertainties in climate simulations might decrease by using km-scale models compared to coarser-resolution models (Ban et al. 2021; Pichelli et al. 2021).

Motivated by the previous studies, the Convection-Permitting Third Pole (CPTP) CORDEX-FPS, was initiated in 2019 to provide high-resolution climate information for the TP region. The main goal of CPTP is to enhance our understanding of the current and future water cycle and its extremes over the TP region. The first phase of the program is to assess the skill of km-scale regional models concerning the simulation of convection, precipitation, and snowfall over the TP region. The second phase will see decadal current and future climate simulation runs within the next three years.

¹ A list can be found here: <https://cordex.org/experiment-guidelines/flagship-pilot-studies/>.

Fig. 1 Topography and computational domains used in the CPTP project. The minimum domain sizes for domain D1 and D2 are shown according to their top-center (TC), right-center (RC), bottom-center (BC), and left-center (LC) points



In this study, we present the results of the first phase of this project. We conducted three reanalysis-driven case experiments that represent important meteorological phenomena associated with the TP - an MCS, a heavy snowfall event, and a Monsoon case—with a multi-model and multi-physics ensemble. The main motivation for these case studies was to set up and test the models in different weather situations over the TP. The simulations were performed over a relatively large common region shown in Fig. 1, with a grid spacing of less than 5 km. Some of the models were run for the first time at such a high spatial resolution over this region. This paper provides an overview of the experimental design and the model performance in simulating precipitation and near-surface air temperature. More detailed analyzes of the presented case study simulations are currently performed and will be published in separate manuscripts.

The objectives of this study are the following:

1. Evaluating various high-resolution models over the TP under various weather conditions and atmospheric processes.
2. Assessing major sources of model performance uncertainties, and
3. Improving the performance of numerical models for future high-resolution climate runs over the TP.

2 Data and methods

2.1 Description of selected cases

We selected three cases for our modeling tests that span a wide variety of atmospheric processes, seasons, and impacts.

2.1.1 MCS—July 2008

MCSs are important features of convective precipitation over the TP (e.g. Sugimoto and Ueno 2010; Kukulies et al. 2021). On July 18, 2008, a mesoscale Tibetan Plateau Vortex (TPV) formed in the western part of the TP, traveled eastward, moved off the TP, and then traveled north-eastward to the coast of the Yellow Sea (Feng et al. 2014; Curio et al. 2019). When the TPV reached the eastern TP, it triggered an MCS at the eastern edges of the TP and produced a substantial amount of convective precipitation in the Yangtze river basin (Kukulies et al. 2021). A station in the Sichuan basin recorded a maximum 24-h accumulated precipitation of 288 mm during this event Feng et al. (2014). The core simulation period for this case is July 14, 2008, 0 UTC–July 24, 2008, 0 UTC.

2.1.2 Monsoon precipitation—August 2014

August 2014 was one of the wettest Augusts in recent decades due to active Monsoon precipitation and embedded extreme precipitation episodes. One particularly intense extreme event led to massive flooding and landslides in western Nepal on August 14–15 2014. During the event, a maximum precipitation amount of 528 mm in 24 h was observed at the Chisapani station (Karki et al. 2018). The core simulation period for this case is July 27, 2014, 0 UTC – September 1, 2014, 0 UTC.

2.1.3 Heavy snow event—October 2018

Climatologically there are two peaks of snow depth over the TP, a maximum in March and a secondary maximum in October. A heavy snow event was recorded at the Institute of Tibetan Plateau Research Nam Co station (30°46.44′N,

90°59.31E, 4,730 m a.s.l.) between October 4–8, 2018 Dai et al. (2020). The purpose of studying the event in October is to cover an extreme event that had been studied in detail by others, rather than to cover a “typical month for snow”. Given the period covered is short and observations are scarce, being able to take advantage of the existing analysis is desirable and useful. This was the largest snowfall event in October since recording began in 2005 at this station. On October 3, 2018, a gust of cold air passed over the group lakes area, causing the daily minimum temperature of the region to drop by about 4.5 °C within 24 h. As a result, the daily minimum temperature reached the freezing point about one week earlier than in previous years. The snowfall to the east of Nam Co was more than 50 cm while it was only 5 cm in the west of Nam Co. The core simulation period for this case is October 1, 2018, 0 UTC—October 9, 2018, 0 UTC.

2.2 Model simulations

The CPTP community agreed on a minimal modeling domain that all modeling experiments have to include (D1 from hereon). The minimum domain size is given not as corner points of a region but as central points to allow for a more efficient design of model domains concerning the employed map projections (Fig. 1). D1 encapsulates the TP region and was selected to minimize the computational cost for running kilometer-scale models. It was recommended to use a coarser resolution parent domain that incorporates a larger region (domain D2) if modelers decided to run their kilometer-scale simulations on D1.

Case study simulations were performed with five modeling systems. An overview of the participating models and their main model settings is shown in Table 1. All simulations downscale the fifth generation ECMWF atmospheric reanalysis (ERA5 Hersbach et al. (2020)) without the application of nudging.

The Advanced Research (AR) Weather Research and Forecasting (WRF) model Skamarock and Klemp (2008); Powers et al. (2017) version 4.2 was used by 9 modelers (see Table 2). WRF is a state-of-the-art mesoscale numerical weather prediction system that is widely used for modeling across weather and climate time scales. WRF uses fully-compressible, Eulerian non-hydrostatic equations that conserve dry air mass and scalar mass. It uses a staggered Arakawa C-grid with a terrain-following, mass-based, hybrid sigma-pressure vertical coordinate system with a vertically stretched grid. WRF features a large range of model physics options. We performed a reference simulation with physics settings that perform well in the U.S. Liu et al. (2017) (see Table 1). The reference simulations are offline nested and initialized from 12 km grid spacing simulations (performed on D2) that started at least 18 months before the case occurrence. The initial and lateral boundary conditions from the

12 km simulations were shared to increase the comparability of WRF sensitivity experiments. Twenty-four, twenty-one, and twelve additional WRF simulations were performed, based on the shared initial and lateral boundary conditions, for the MCS, Snow, and Monsoon cases, respectively. Two of these simulations reproduced the reference run on a different high-performance computer (HPC) system to understand sensitivities to HPC architectures. The other simulations subsequently perturbed the planetary boundary layer (PBL) scheme, microphysics scheme, land surface model (LSM), applied a scale aware cumulus scheme, or performed a time-lagged ensemble to estimate the effect of natural variability on the MCS case. For an overview of the simulation names and perturbed physics see Table 2 where gray cells indicate that the settings are the same as in the reference run while red cells show settings that have been changed. Two additional simulations are performed where one uses the reference physics set up and runs the 4 km WRF simulation on D2 by directly downscaling ERA5 and the second repeats the reference simulation over D1 but directly downscaling ERA5 instead of using the 12 km run data. Although we do not see strong spin up effects due to the large grid spacing difference between ERA5 and WRF in our simulations, previous studies documented that large grid spacing differences can deteriorate the regional model results (Matte et al. 2017).

The Model for Prediction Across Scale (MPAS) is a modeling framework to numerically solve the equations of geophysical fluid dynamics (Ringler et al. 2010, 2013). Currently, four MPAS models have been developed to simulate different components of the climate system: atmosphere, ocean, sea ice, and land ice (<http://mpas-dev.github.io/>). The MPAS-Atmosphere solves fully compressible, non-hydrostatic equations of mass, momentum, and energy conservation for the atmosphere (Skamarock et al. 2012). MPAS shares many aspects of its numerical scheme (e.g., time integration and numerical damping) Park et al. (2014) and physics parameterizations with the WRF model (Duda et al. 2019). The distinct features of the MPAS model are the global unstructured mesh on a sphere (Spherical Centroidal Voronoi Tessellations (SCVT), (Ringler et al. 2010; Ju et al. 2011), the C-grid finite-volume scheme designed for the SCVT mesh, and a new terrain-following vertical grid (Klemp 2011). The SCVT mesh can be configured as a global quasi-uniform resolution mesh and as a variable-resolution (VR) mesh in which grid spacing smoothly transitions from the refined to the coarse domain. The SCVT can also be set up as a regional grid, making it possible to compare the global and limited-area modeling approaches within one modeling framework (Skamarock et al. 2018), which is the approach taken here.

For this study, we use the MPAS-Atmosphere version 7.0 and a global variable-resolution SCVT grid, on which

the grid spacing smoothly changes from ~ 4 km over TP to ~ 32 km over the rest of the globe. A predefined convection-permitting physics parameterization suite, which includes a scale-aware parameterization scheme for convection, is used (Table 1). The global VR mesh does not need lateral boundary conditions, therefore only the daily-mean sea surface temperature and sea ice fraction are prescribed from ERA5, and input to the model once a day. For the MCS case, two additional global VR simulations are performed using time-lagged initial conditions (ERA5 state at 6 and 12 hours before the initial time, same as those of the WRF initial condition ensemble). A regional SCVT grid is also produced by extracting the high-resolution domain from the global 4–32 km grid. For this work we limit our analysis of the limited-area simulation to the MCS case, because the regional MPAS simulation over TP experiences stronger numerical instabilities than in the global VR simulation and an optimal configuration of the regional SCVT over TP is being tested at the time of writing. For the limited-area simulation, 6-h lateral boundary conditions are prescribed from ERA5, and a shorter model time step than the global VR is used (12 s vs. 24 s). All the other configurations are identical between the global and limited-area MPAS simulations.

Another modeling group employed the COSMO (Consortium for Small Scale Modeling) model run in climate mode (COSMO-CLM, hereafter CCLM; Rockel et al. (2008), Baldauf et al. (2011)). CCLM is a non-hydrostatic, fully compressible, limited-area model, which similarly to the WRF and MPAS model employs an Arakawa C-grid and a terrain-following vertical coordinate with a user-defined stretched grid. The simulations employed the accelerated version of CCLM, which has been refactored to exploit heterogeneous node architectures Fuhrer et al. (2014) and provides a $\sim 5\times$ speed-up compared to the version that only runs on central processing units. The model was configured with a 12-km parent domain and a 2.2-km grid spacing child domain, the latter of which encompassed the extent of D2 (cf. Fig. 1). Initial and lateral boundary conditions for the 12-km domain were provided at 6-hourly intervals from the ERA5 reanalysis, while the 2.2-km domain was run offline with lateral boundary conditions updated hourly from the parent domain. CCLM has been used extensively for kilometer-scale climate simulations over the European Alps (e.g., Ban et al. 2014, 2021) and was applied over High Mountain Asia for the first time for these simulations using similar options for the model configuration and physics. A few settings were changed to improve model stability over the complex orography, including using a different upper boundary condition and introducing cold-pool diffusion in the 2.2-km domain.

The Icosahedral Nonhydrostatic model (ICON) is a unified next-generation global numerical weather prediction and climate modeling system Zängl et al. (2015), and was used by two modeling groups (see Table 2) in this study. The

ICON model was co-developed by the Max Planck Institute for Meteorology and the German Weather Service. The dynamical core of ICON is formulated on an icosahedral-triangular Arakawa C grid. It has a height-based vertical coordinate system with terrain following layers at the surface. For this study, one simulation used the ICON model version 2.6.1, while the other 2.6.3 in its operational numerical weather prediction mode. The limited-area simulations were performed on D1 for one simulation, and on the domain represented with light blue color in Fig. 1 for the other simulation. The horizontal resolution for both the simulations was about 3.3 km. The deep convection parameterization was switched off for both the simulation runs, while a shallow convection scheme is switched on for one of the simulations. Other details of the ICON model settings are summarized in Table 1. The ICON simulations were forced with initial and lateral boundary conditions directly from the ERA5 reanalysis at 3-h intervals for one simulation, and 1-hourly intervals for the other simulation. The ICON simulations were completed on the Chinese Earth System Science Numerical Simulator Facility “EarthLab” and on Goethe-HLR HPC cluster at the Goethe University Frankfurt.

Last but not least, the Regional Climate Model version 4 (RegCM4) is developed and maintained at the Abdus Salam International Centre for Theoretical Physics (ICTP) in Italy Giorgi et al. (2012); Coppola et al. (2021) was also utilized. The standard version of RegCM4 with hydrostatic dynamics is a widely used system that has been applied to local and regional seasonal forecasting and climate change studies for all regions of the globe, including the TP region (e.g., Sanjay et al. 2017; Wang et al. 2021). The CPTP case study experiments are performed with a development version 4.8.0 of RegCM4 model with non-hydrostatic dynamics Coppola et al. (2021). The initial and 6-hourly lateral boundary conditions and sea surface temperature for the 4 km simulations on D2 are directly derived from ERA5. The model has a wide choice of physical parameterizations for processes such as non-convective clouds and resolved-scale precipitation, land surface models, planetary boundary layer turbulent diffusion, ocean surface fluxes etc. Giorgi et al. (2012); Coppola et al. (2021). The physics options adopted for the CPTP experiments are summarized in Table 1. The land surface processes are described using the Biosphere -Atmosphere Transfer Scheme (BATS; Dickinson (1993)). The resolved-scale cloud microphysics is treated by a simple subgrid explicit moisture scheme (SUBEX, Pal et al. (2000)), which has only one prognostic equation for calculating cloud water content based on autoconversion of cloud water to rainwater, accretion of rainwater, and evaporation of raindrops. The cloud fractional cover is diagnostically calculated as a function of grid point average relative humidity. SUBEX does not treat cold cloud microphysics and the fraction of ice is diagnosed as a function of temperature in the RegCM4

radiation scheme from radiative transfer calculations Giorgi et al. (2012).

2.3 Observations

The TP region is an observationally sparse area with a harsh environment that introduces large observational uncertainties. To account for these uncertainties, we use an ensemble of in situ, remote-sensing, and reanalysis-based precipitation and near-surface temperature datasets that provide data on daily or higher resolution.

For precipitation, we use the CHIRPS Funk et al. (2015), GPM-IMERG Huffman et al. (2015), CPC Xie et al. (2010), APHRODITE (Yatagai et al. 2012), and ERA5 Hersbach et al. (2020) datasets. The Climate Hazards group Infrared Precipitation with Stations (CHIRPS) dataset uses infrared satellite observations blended with station data to create a quasi-global (50°S–50°N), 0.05° grid spacing, daily precipitation estimate. NASA's Global Precipitation Measurement (GPM) Integrated Multi-satellitE Retrievals for GPM (IMERG) product intercalibrates, merges, and interpolates all available satellite microwave precipitation estimates, microwave-calibrated infrared satellite estimates, and precipitation gauge observations on a global 0.1° grid every 30-minutes. NOAA Climate Prediction Center (CPC) daily precipitation estimates combine over 30,000 gauges to create a global, land-only gridded product with 0.5° spacing. The Asian Precipitation-Highly Resolved Observational Data Integration Towards Evaluation of Water Resources (APHRODITE) dataset incorporates 5,000–12,000 precipitation stations to create a 25 km × 25 km gridded dataset with daily precipitation accumulations. We leverage the monsoon Asia version of APHRODITE in this study (APHRO_V1101EX_R1/), which provides data from 2007 to 2015. ERA5 uses data assimilation to combine a large variety of in-situ and remote sensing observations with forecasts from an advanced global model to create an estimate of the global atmospheric state. Data is provided hourly on a global 30 km grid.

Gridded precipitation datasets that are based on or calibrated with gauge data typically feature an underestimation of precipitation that stems from two primary sources. First, gauges undercatch precipitation particularly in exposed and snow-dominated environments Prein and Gobiet (2017). Second, precipitation gauges are typically located in valleys and not on mountain slopes. This results in a sampling bias of precipitation values since precipitation has a complex altitude dependence in the Himalayas region Singh and Kumar (1997). To account for these biases, we apply monthly bias correction estimates from Beck et al. (2020). These estimates are based on water budget calculations taking into account precipitation, runoff, and evaporation using 9372 streamflow stations

worldwide. Satellite precipitation estimates have difficulties in observing precipitation in snow dominated regions and frequently have large errors over high-mountain regions (Lu et al. 2019; Sharma et al. 2020). Precipitation estimates based on satellite remote sensing data, such as GPM-IMERG, can have deficiencies that are particularly large in mountain regions since satellite radars can not see all the way to the surface due to ground clutter, microwave precipitation estimates are masked out over snowy/icy surfaces, and ground observations for precipitation calibration are fewer in complex topography (Bartsotas et al. 2018; Huffman 2019).

For near-surface temperature, we again use ERA5 and CPC data in addition to GLDAS Rodell et al. (2004) and Berkeley Earth Rohde et al. (2013) observations. The Global Land Data Assimilation System (GLDAS) merges ground-based and satellite observational data with advanced land surface modeling techniques. GLDAS provides 3-hourly data on a 0.25° global grid. The Berkeley Earth dataset combines station observations with an algorithm that is optimized for climate change assessments and provides daily data on a 1° global, land-only grid. All gridded observational datasets and model outputs are bi-linearly interpolated to the ERA5 grid for model evaluation.

We decided to use GPM-IMERG as reference for precipitation analysis and GLDAS for T2M analyses and use these to show differences to other observational and model data. Using GPM-IMERG and GLDAS as references is subjective and any of the other observational datasets could be used instead. The main reason why we chose these two datasets is that they merge large amounts of information including satellite and model information, their high spatiotemporal resolution, and the data availability for all cases.

In addition to these gridded datasets, we also use Hadley Center Integrated Surface Database (HadISD) sub-daily station observations for model validation Dunn et al. (2016). Global sub-daily station records are collected from the stations that meet specific selection criteria and a suite of quality control tests are performed. The location of all stations within the HadISD dataset is shown in Supplementary Fig. S1. Hourly temperature data and 6-hourly precipitation accumulations are compared to model output from the nearest native model grid cell if there are at least 30 % valid observations during the evaluation period. Choosing this low level of completeness is necessary to include stations on the TP, which often have many missing values in their record. Time steps that are missing in the observational record are also set to missing values in the modeled time series for consistency. Using inverse distance averaging of the four closest model grid cells leads to similar results.

2.4 Methods

The analysis of modeling uncertainties is performed similarly to Rowell (2006). Therefore, we classify different sources of uncertainty for which simulations are available in the CPTP case study ensemble. We investigate three general classes of uncertainty—model formulation uncertainty, observational uncertainty, and initial condition uncertainty—and six classes that are specific to the WRF model ensemble—PBL scheme, microphysics, LSM, convection scheme, domain size, and high-performance computing system sensitivity. Uncertainties are estimated by averaging over all categories, except the one under consideration, and calculating the standard deviation over the data points in the considered category. For instance, model formulation uncertainties are estimated by averaging over all available simulations from a particular model. This results in one data point per model, which is used in the calculation of the standard deviation.

The model formulation uncertainty stems from differences in the assumptions and equations used in the participating climate models. The observational uncertainties are estimated by comparing different gridded observational products with each other. The initial condition uncertainty addresses the chaotic nature of the simulated cases, which arises from constructing a time-lagged initial condition ensemble. This has only been done for the MCS case with WRF and MPAS, but we expect the results to be similar for other modeling systems and cases. PBL, microphysics, LSM, and convective scheme uncertainties are estimated from the WRF physics sensitivity studies. The domain size uncertainty is estimated by running WRF simulations on D1 and D2, while HPC system sensitivities are calculated from running the same WRF setup on different computer architectures.

The Rowell (2006) method of estimating uncertainties is beneficial due to its simplicity and easily interpretable results. However, it might result in unreliable uncertainty estimates for categories that are sparsely populated (e.g., convection scheme uncertainties) and does not account for effects from interactions between categories (e.g., PBL scheme impacts on simulations on different domain sizes).

Even though most of the simulations are run with the same horizontal grid spacing of 4 km, the modeling systems may vary in their effective resolution and capability to resolve deep convective processes, i.e. due to differences in the numerical schemes Skamarock (2004), Zeman et al. (2021). To get an indication of how well kinetic energy (KE) is retained at different spatial scales in the used models, we inter-compare KE power spectra based on horizontal wind speeds at 500 hPa and 200 hPa. The python package *scipy*.*fftpack* (<https://docs.scipy.org/doc/scipy/reference/generated/scipy.fftpack.dctn.html>) is used to compute spectral

coefficients from 3-h two-dimensional wind fields applying a discrete cosine transformation (Denis et al. 2002). The power spectra were constructed by calculating the variances of these spectral coefficients for specific wavelength bins, following the steps in Denis et al. (2002). Note that all model output was first reduced to the domain D1 (Fig. 1) since the offset of the KE spectra is domain-sensitive.

3 Results

This section presents results from the analysis of kinetic energy (Sect. 3.1), precipitation (Sect. 3.2), near-surface temperature (Sect. 3.3), and the analysis of uncertainty sources (Sect. 3.4).

3.1 Spectral analysis

Although the grid spacing of the five participating modeling systems is similar, their ability to simulate fine-scale atmospheric dynamics might be different due to different choices in how to solve the equations of motion and how diffusive the models are Zeman et al. (2021). Figure 2 shows power spectra of horizontal kinetic energy at 500 hPa (a) and 200 hPa (c) for the participating modeling systems (UIBK-CCLM50n, rli2p1_NCAR-WRF42, rli1p1_PNNL-MPA-SLA7, IAP-ICON2.6, GUF-ICON2.6.3, IITM-RegCM480) and their driving reanalysis ERA5 based on hourly data from the 10-day long MCS case simulation (the spectra for the other cases look very similar—not shown). The KE spectra for the simulations converge well with ERA5 at higher wavelengths, where kinetic energy shows the largest variability, and spatial features are expected to be similar because they are mainly produced by the large-scale circulation. The km-scale simulations retain more energy at the small wavelengths compared to ERA5 and the 12 km simulations that served as parent simulations for nested runs with WRF and CCLM. This maintenance of kinetic energy can be attributed to the higher effective resolution in the km-scale simulations and to the fact that deep convection is not parametrized, as shown in Zeman et al. (2021) (Zeman et al. 2021).

The gray lines in Fig. 2a-d indicate theoretical slopes derived from observations (Nastrom et al. 1984) that describe the energy loss at synoptic (k^{-3}) and mesoscales ($k^{-5/3}$) as a function of wavenumber k . These can be compared to the actual spectral slopes for the KE spectra in Fig. 2c-d. It is discernable that the simulated slopes at 500 hPa are shallower than the expected slope for mesoscales, while the slopes at 200 hPa show closer resemblance to the expected slopes for synoptic and mesoscales. For wavelengths around 1,000 km, most of the KE spectra exhibit slopes similar to k^{-3} . The slopes become shallower and more similar to $k^{-5/3}$ at around 400 km, which is a

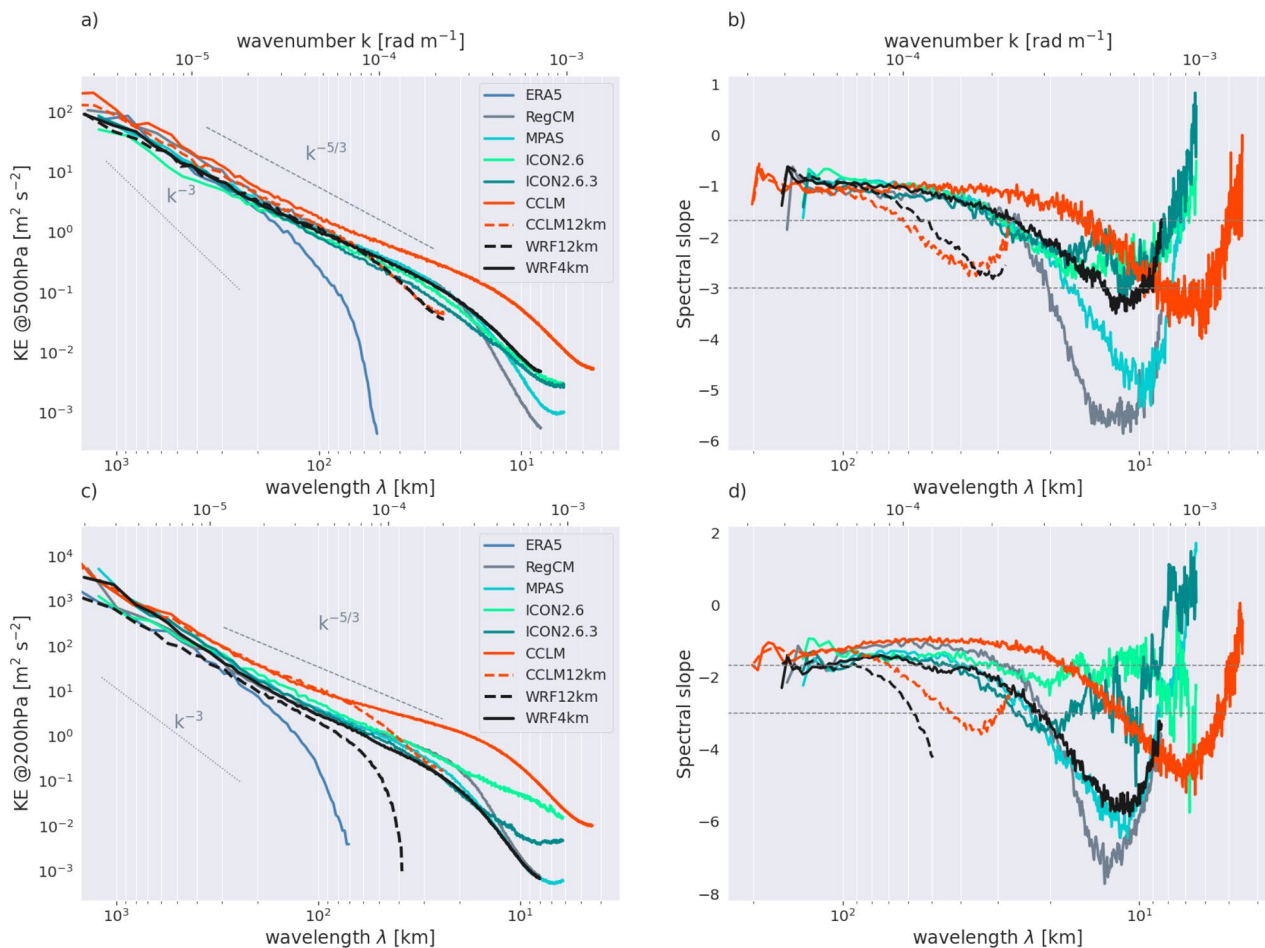


Fig. 2 Power spectra of horizontal kinetic energy [$\text{m}^2 \text{s}^{-2}$] at 500 hPa (a) and 200 hPa (c) and corresponding spectral slopes (b, d) as a function of wavenumber [k rad^{-1}] and wavelength [km]. The power spectra are com-

puted using the extent of the domain D1. Spectral slopes are high-pass filtered using a moving average to reduce noise. The gray lines mark the theoretical slopes for synoptic (k^{-3}) and meso-scale ($k^{-5/3}$) energy loss

typical transition zone between synoptic and mesoscale (e.g. Zeman et al. 2021). The shallower slope at 500 hPa compared to 200 hPa is likely caused by the complex terrain that covers most of the domain (Fig. 1) and is strongly affecting the flow at 500 hPa. As pointed out by Skamarock et al. (2014) (Skamarock and Klemp 2008) and Blažica et al. (2013), topography can have considerable effects on divergent kinetic energy, for example through the generation of gravity waves or other topographic flow interactions.

Comparing the 12 km simulations from CCLM and WRF with their respective higher resolution runs at 2.2 km and 4 km grid spacing, it can be seen that the KE spectra start to diverge at wavelengths of ~ 50 km at 500 hPa and ~ 70 km at 200 hPa. This abrupt loss in KE energy can be interpreted as the effective resolution of the models, which is also reflected in the energy drop at ~ 20 km in the 4 km WRF simulation and at 10 km in the

2.2 km CCLM simulation. For WRF and CCLM, this corresponds to an effective resolution of about $4\text{--}6 \Delta x$. The KE spectra for MPAS look similar to those of WRF, even though MPAS tails off slightly earlier for kinetic energy at 500 hPa. These results are consistent with Skamarock et al. (2014), who demonstrated that global MPAS simulations produce an effective resolution of about $6 \Delta x$. The reason for RegCM4's premature loss in energy at ~ 20 km is not clear since the model uses a relatively short time step, which should be beneficial for the maintenance of high-frequency waves Zeman et al. (2021). While ICON's spectra look similar to WRF at 500 hPa, it maintains a k^{-3} slope until very small wavelengths at 200 hPa. While the KE spectra for ICON2.6 and ICON2.6.3 look similar at 500 hPa, they diverge from wavelengths smaller than 200 km at 200 hPa. The exact cause of these differences is unclear since the two simulations differ in model version, time step, domain size, and model physics (Table 1).

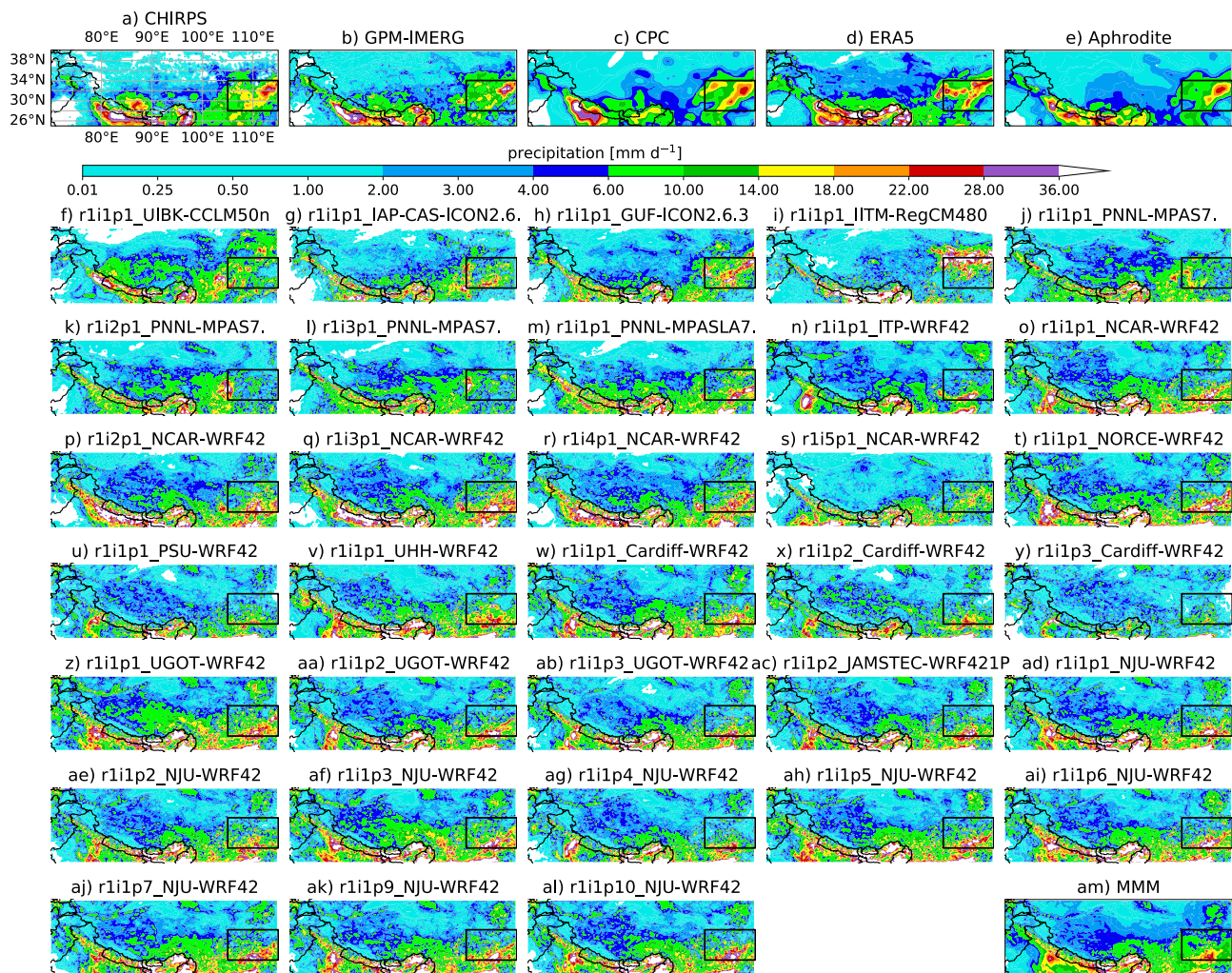


Fig. 3 Average daily precipitation from the MCS case during July 16–23, 2008. The top row (a–d) shows various gridded observational datasets and rows below show the model simulated precipitation.

The multi-model mean (MMM) is shown in (e). The black rectangle shows the approximate region of heavy precipitation that was caused by the MCS event

The spectrum for ICON2.6.3 agrees more with WRF and MPAS for wavelengths > 200 km.

The different physics options within the WRF ensemble do not substantially affect the KE spectra (not shown), but the small differences between MPAS and WRF4km at 500 hPa for smaller wavelengths might be partly caused by the use of a scale-aware convective parameterization scheme in MPAS, while convection is explicitly simulated in the WRF simulations (Table 1).

3.2 Precipitation analyses

Here we evaluate the accuracy of simulated precipitation against a range of observational products. The goal is to provide an overview of the models' skill in capturing key features such as spatial precipitation patterns, precipitation accumulations over time, and 6-hourly precipitation rates.

Fig. 3 shows the average precipitation during the MCS case in July 16–21, 2008. Flood-producing rainfall was produced by the MCS in the Chinese province of Sichuan and heavy rainfall was also reported in the southern foothills of the Himalayas. All observational datasets (Fig. 3a–d) show a precipitation maximum at $\sim 115^\circ$ east and $\sim 30^\circ$ north, which varies in spatial extent and intensity between the datasets. Only the GUF-ICON2.6.3 simulation (Fig. 3h) was able to capture the exact location of the MCS precipitation. Most simulations have a precipitation maximum that is displaced towards the south or miss the MCS precipitation completely. The RegCM4 simulation is the only run that has a northward displacement of the precipitation center (Fig. 3i). The precipitation along the southern foothills of the Himalayas is accurately simulated in most models. Kukulies et al. [93] shows that the southward displacement of the MCS precipitation in most models is primarily caused by

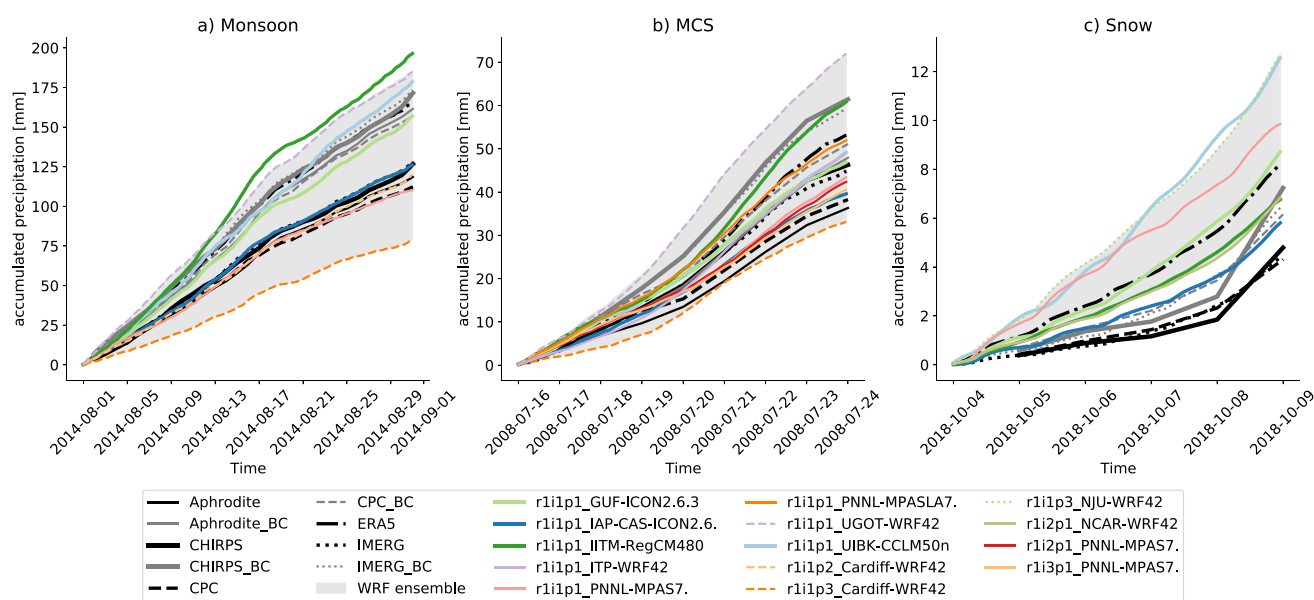


Fig. 4 Domain average accumulated precipitation during the Monsoon (a), MCS (b), and Snow (c) case experiment. Black lines show various observational datasets, gray lines show bias corrected observational datasets following Beck et al. (2020), and colored lines show

simulated precipitation. The gray contour shows the WRF ensemble spread. Only the WRF simulation with the lowest absolute difference compared to IMERG and with the lowest and largest precipitation accumulation are shown

biases in simulating jet stream interactions with the TPV. Differences between the simulated event average and the GPM-IMERGB precipitation can be seen in Supplementary Fig. S2. The amount and spatial distribution of event average precipitation is well captured by most models for the Monsoon case (Supplementary Figs. S3 and S4) while most models show more precipitation during the Snow case in the eastern foothills and on the Tibetan Plateau (Supplementary Fig. S5 and S6).

The domain-averaged accumulated precipitation for all three cases is shown in Fig. 4. For the Monsoon case (Fig. 4a), the observational datasets agree well when the precipitation correction of Beck et al. (2020) is applied. The ERA5 precipitation, which does not suffer from undercatch and sampling biases, is much higher than the one from station-based datasets if the correction is not applied. The WRF ensemble has a large spread of accumulations that encompasses all observational datasets and all simulations from other modeling systems, except for those from the RegCM4 model. The source of this spread will be explored in a later section. The simulations with the MPAS and ICON model are similar to the not bias corrected observational datasets, while precipitation in the CCLM and RegCM4 simulations is comparable to the bias-corrected version of these datasets and ERA5 precipitation.

The results from the domain average accumulated precipitation during the MCS case (Fig. 4b) are similar to the Monsoon case. Again, the WRF ensemble spread is large and encompasses the observational datasets and other

model simulations. The simulated precipitation is overall centered on the observed precipitation, which is in part due to compensating errors in the spatial representation of precipitation (e.g., see Fig. 3). The largest differences between observational and modeled precipitation can be found in the Snow case (Fig. 4c). Here, the models tend to simulate much higher precipitation accumulations and the WRF ensemble does not bracket the other models, nor the observational datasets, even after bias correction.

To assess the models' performance in simulating precipitation patterns we show the event-averaged precipitation pattern correlation coefficients, standard deviation, and centered root mean square error in Taylor diagrams Taylor (2001) (Fig. 5). Modeled correlation coefficients are between 0.63–0.82 (except for r1i1p3_Cardiff-WRF42) for the Monsoon case (Fig. 5a), 0.3–0.65 for the MCS case (Fig. 5b), and 0.22–0.5 for the Snow case (Fig. 5c). The differences between the cases are not only due to the models' ability to capture precipitation under different atmospheric settings but are also a result of uncertainties in observational datasets. Most models have larger spatial variability (i.e., standard deviations) than the observational datasets, particularly during the Snow case. This is in part due to the higher effective resolution of the kilometer-scale simulations compared to the observational datasets. The best performing simulations according to this metric are the GUF-ICON2.6.3 simulations, PNNL-MPAS7 runs, the IAP-CAS-ICON2.6 simulation, and the WRF simulations that directly downscale ERA5 data over the larger domain

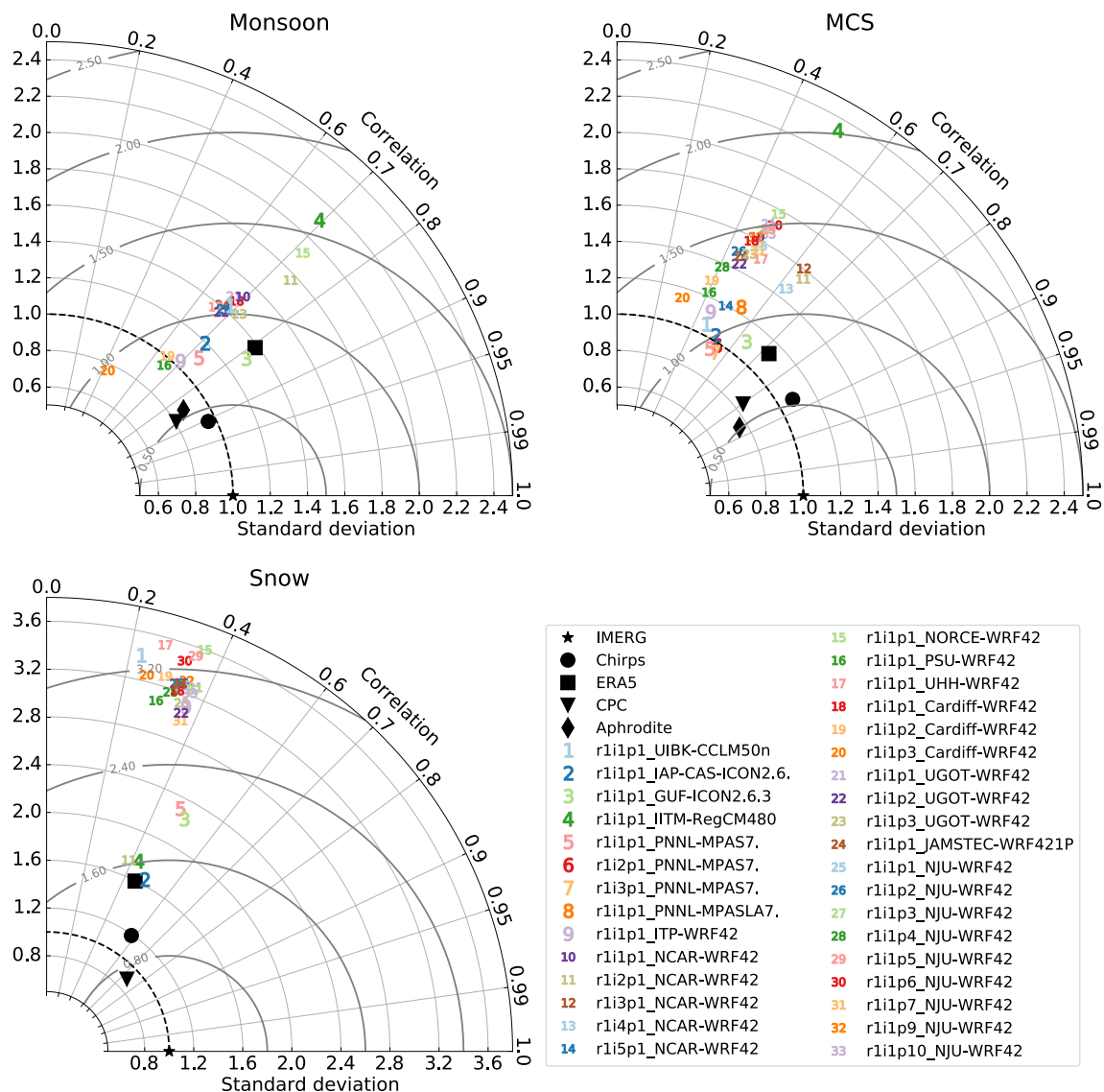


Fig. 5 Taylor diagrams showing the case average precipitation pattern correlation, spatial standard deviation, and centred root mean square error comparing observational (black symbols; non-bias corrected) and modeled precipitation (colored numbers) with IMERG observations

D2 (r1i2p1_NCAR-WRF42). The r1i1p3_Cardiff-WRF42 run is an outlier concerning the low correlation coefficients in all cases suggesting that the combination of the MYNN3 PBL scheme and the WDM7 microphysics results in sub-par model performance. Interestingly, using the schemes separately such as in r1i1p2_Cardiff-WRF42 and r1i1p3_UGOT-WRF42 does not deteriorate the simulations. The IITM-RegCM480 simulations are outliers due to their high spatial variability during the Monsoon and MCS case.

The simulations can capture the gauge-based 6-h precipitation probability density functions well (Fig. 6) and outperform the ERA5 precipitation, which overestimates weak precipitation frequencies and underestimates high precipitation frequencies. The WRF ensemble spread encompasses

most of the other model solutions. The IMERG precipitation accumulations agree well with those from the stations except for the Snow case, which has large observational uncertainties.

The correlogram in Fig. 7 provides insights into the similarity of case average spatial precipitation accumulation patterns. The upper left corner of the correlograms shows the correlation coefficients comparing the observational datasets. Overall, correlation coefficients are high, indicating good agreement between the observed spatial precipitation patterns. The lowest correlation coefficients can be found for the Snow case confirming the previously discussed observational uncertainties. Bias correcting the observational datasets (indicated by a `_BC` at the end of the

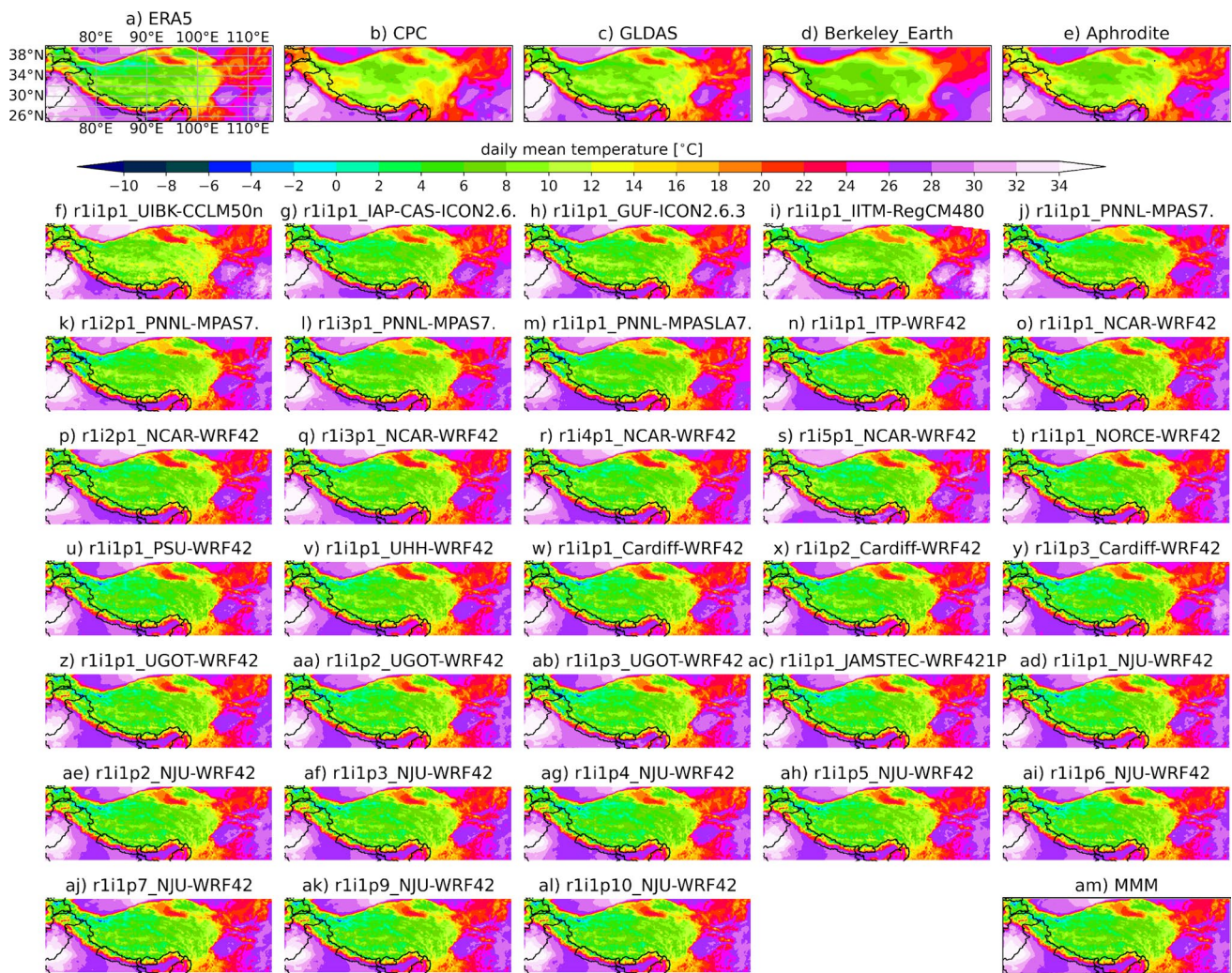


Fig. 8 Average daily mean 2 m above surface air temperature for the MCS case during July 16–23, 2008. The top row (a–d) shows various gridded observational datasets and rows below show the model simulated T2M

r1i3p1_NCAR-WRF42, r1i4p1_NCAR-WRF42) independent of the observational dataset.

The correlation coefficients between the WRF ensemble and the other model simulations (middle horizontal block) are comparable to the coefficients obtained when comparing the models to the observations. Precipitation patterns from most WRF simulations (rightmost block) are highly correlated, indicating that there is little sensitivity to changing the model physics. Notable exceptions are the r1i1p3_Cardiff-WRF42 simulation, which uses the MYNN3 PBL and WDM7 PBL scheme, and the large domain WRF simulations that directly downscale ERA5 (r1i2p1_NCAR-WRF42, r1i3p1_NCAR-WRF42, r1i4p1_NCAR-WRF42).

3.3 Two meter above ground air temperature analysis

This section presents a similar analysis as the previous section but for T2M. Figure 8 shows the July 16–23, 2008 average T2M for the MCS case from the observational datasets (Fig. 8a–d) and the model ensemble (Fig. 8e–al). As expected, T2M strongly depends on topography with very warm temperatures in India and south-eastern China and substantially colder temperatures over the TP. The observational datasets agree reasonably well concerning the large-scale pattern of T2M but cool differences over the TP and warm differences in the eastern part of the domain compared to the GLDAS data are present in the MCS and Monsoon

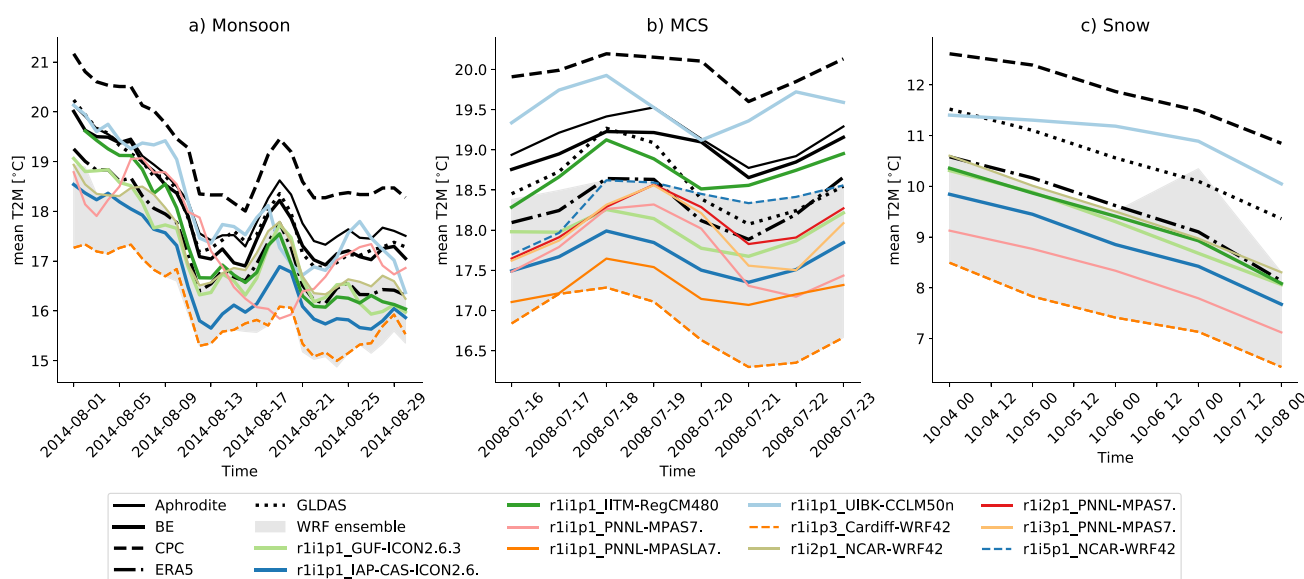


Fig. 9 Domain average daily mean T2M during the Monsoon (a), MCS (b), and Snow (c) case experiment. Black lines show various observational datasets and colored lines show simulated T2M. The

gray contour shows the WRF ensemble spread. Only the WRF simulation with the lowest absolute difference compared to GLDAS and with the lowest and largest T2M values are shown

case (see Supplementary Fig. S7 and S9). Large uncertainties exist on regional scales (see Supplementary Fig. S6, S8, and S10). The simulations are generally able to capture the spatial pattern of T2M but similar differences as discussed above with too cold temperatures over the TP and warm differences east of the TP in the MCS and Monsoon case are visible (Supplementary Fig. S6, S8, and S10). The most noticeable difference is found in the UIBK-CCLM50n run, which has a warmer T2M over the plateau than other simulations agreeing with the CPC observations. T2M differences for the Monsoon and Snow case are similar to the MCS case with UIBK-CCLM50n generally simulating the warmest temperatures over the plateau and WRF simulating the coldest (particularly during the Snow case; see Supplementary Fig. S8–S11).

The domain D1 average daily T2M time series are shown in Fig. 9. The temporal evolution of temperature is well captured by most models but many modeling systems, except for CCLM and RegCM, simulate lower T2M than found in the observational datasets, which is similar to the ERA5 forcing data.

Hourly T2M probability density functions from station observations show a left-skewed (i.e., cold temperature) distribution which is caused by stations on the Tibetan Plateau (Fig. 10). This is most noticeable during the Snow case, which features a cold air outbreak over the plateau. Most simulations can capture the observed PDFs well except for the r1i1p1_PNNL-MPAS7 Monsoon and the r1i1p2_Cardiff-WRF42 Snow simulations. The differences in the MPAS run are likely due to the global nature of this simulation,

which allows it to drift from the observed weather during the month-long simulation. Additionally, the IITM-RegCM480 runs also exhibit noticeable differences in the left tail of their PDF.

Case average T2M spatial correlation coefficients are larger than 0.95 comparing the observational and model datasets to GLDAS (Fig. 11). Interestingly, the Snow case has the highest correlation coefficients between the observational and modeled datasets, indicating that previously shown differences in Fig. 9c are primarily caused by systematic (domain-wide) T2M biases that do not affect pattern correlation coefficients substantially. The high pattern correlation coefficients are primarily caused by the dominant role of topography on T2M.

The vertical distribution of T2M differences compared to station data is shown in Fig. 12. Most of the stations above 2000 m are on the Tibetan Plateau. Temperatures are better simulated at elevations below 2000 m, and most models have a cold bias at higher elevations. Exceptions are the CCLM simulations and the r1i1p1_PNNL-MPAS7 Monsoon case run. The largest cold biases above 2000 m are found in the RegCM4 simulations, particularly during the Snow case.

3.4 Uncertainty sources

In this section, we estimate the sources of model performance uncertainties in simulating case-average precipitation and T2M patterns and amounts (see method section for more details). We use the GPM-IMERG and GLDAS observations as ground truth. However, using different datasets

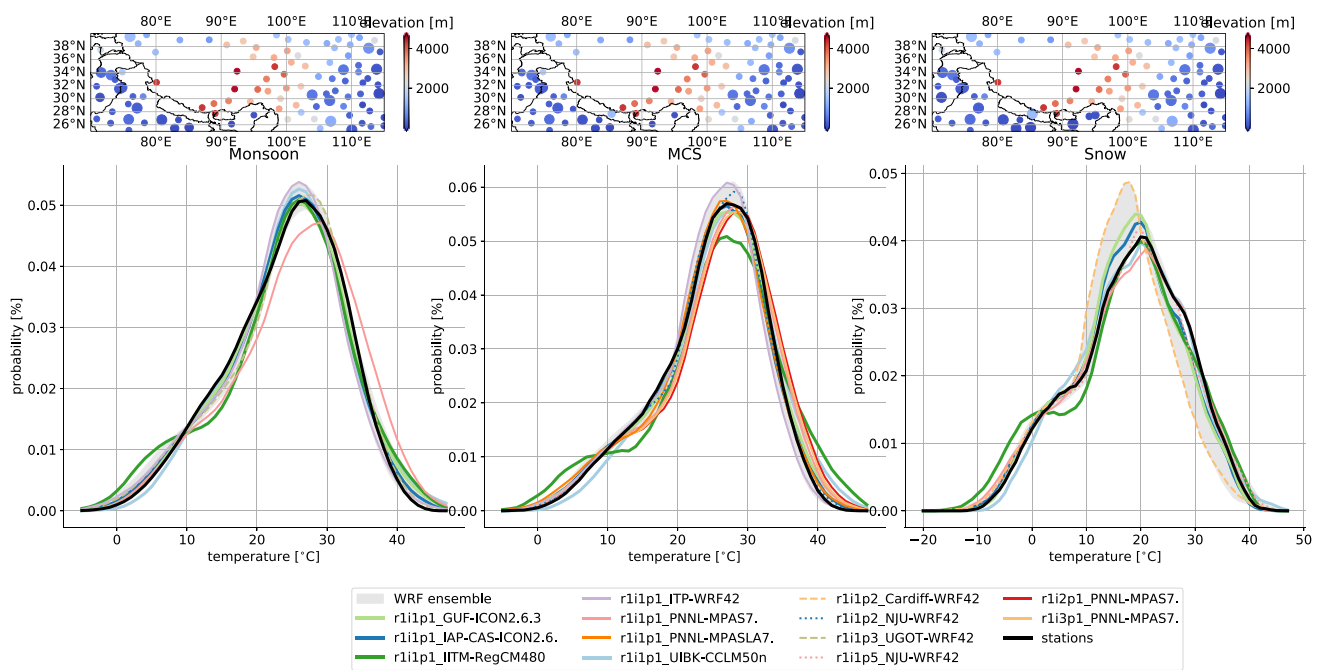


Fig. 10 Probability density function (PDF) of hourly T2M observations from the HadISD station dataset (thick black line) with ERA5 (dotted black line), IMERG (black dashed line), and modeled data (colored lines). The map on top of each panel shows the station locations, station altitude (colors), and completeness of record (circle size; only stations with more than 30 % of valid data are consid-

ered). Gray contours show the WRF ensemble spread. Additionally, the WRF simulation with the lowest absolute PDF difference and the largest PDF difference are shown. The bin size to calculate PDFs is 1 °C and we use a ± 2 °C window around each bin to reduce noise in the PDF calculation

as references does not change the main conclusions on the sources of model uncertainties but they can affect the ranking of modeling systems.

For instance, we derive the pattern correlation coefficient for the case average precipitation between the observational datasets compared to GPM-IMERG and calculate the standard deviation of the resulting correlation coefficients. This gives us an estimate of observational uncertainties (Fig. 13a). This uncertainty estimate can be directly compared to other sources of uncertainty as introduced in the methods section.

Differences in gridded observational datasets are the largest source of uncertainties for all cases and statistics except for absolute differences in precipitation where differences in the model formulation are larger (Fig. 13). This highlights the challenges of constraining observational fields in the TP region. The model formulation standard deviations are of similar magnitude for all cases except for a larger spread in correlation coefficients during the Snow case (Fig. 13a) and a larger spread in absolute precipitation differences during the MCS case (Fig. 13b). The ICON simulations show the overall highest skill in simulating the precipitation statistics. MPAS runs come in as a close second, which is remarkable since the global MPAS simulations are not constrained by ERA5 lateral boundary conditions and have a much larger

degree of freedom to deviate from observed weather patterns compared to the regional models. Differences in T2M correlation coefficients are much smaller than for precipitation and the RegCM4 simulations perform best when it comes to capturing T2M statistics (Fig. 13c). The ensemble average WRF statistics are sub-optimal, however, WRF can be configured to perform equally well as other modeling systems as can be seen when looking at the physics sensitivity results.

Varying initial conditions by creating a time-lag ensemble causes very small uncertainties in the MCS case using the WRF and MPAS model. This indicates that differences between e.g., modeling systems or WRF physics schemes are robust and are not heavily affected by chaotic variability for the MCS case. We expect similar results for the Snow case, which has a comparable runtime to the MCS case, but internal variability might be larger during the Monsoon case due to the longer integration.

The large number of WRF simulations allows us to estimate sources of uncertainties due to different model physics. It should be noted that not all available WRF physics options were tested (we focused on the most popular and up-to-date schemes) and that the selection of tested model physics affects the results. Three institutes ran WRF simulations using the reference settings (see Table 1) from which we can assess uncertainties from running WRF on different

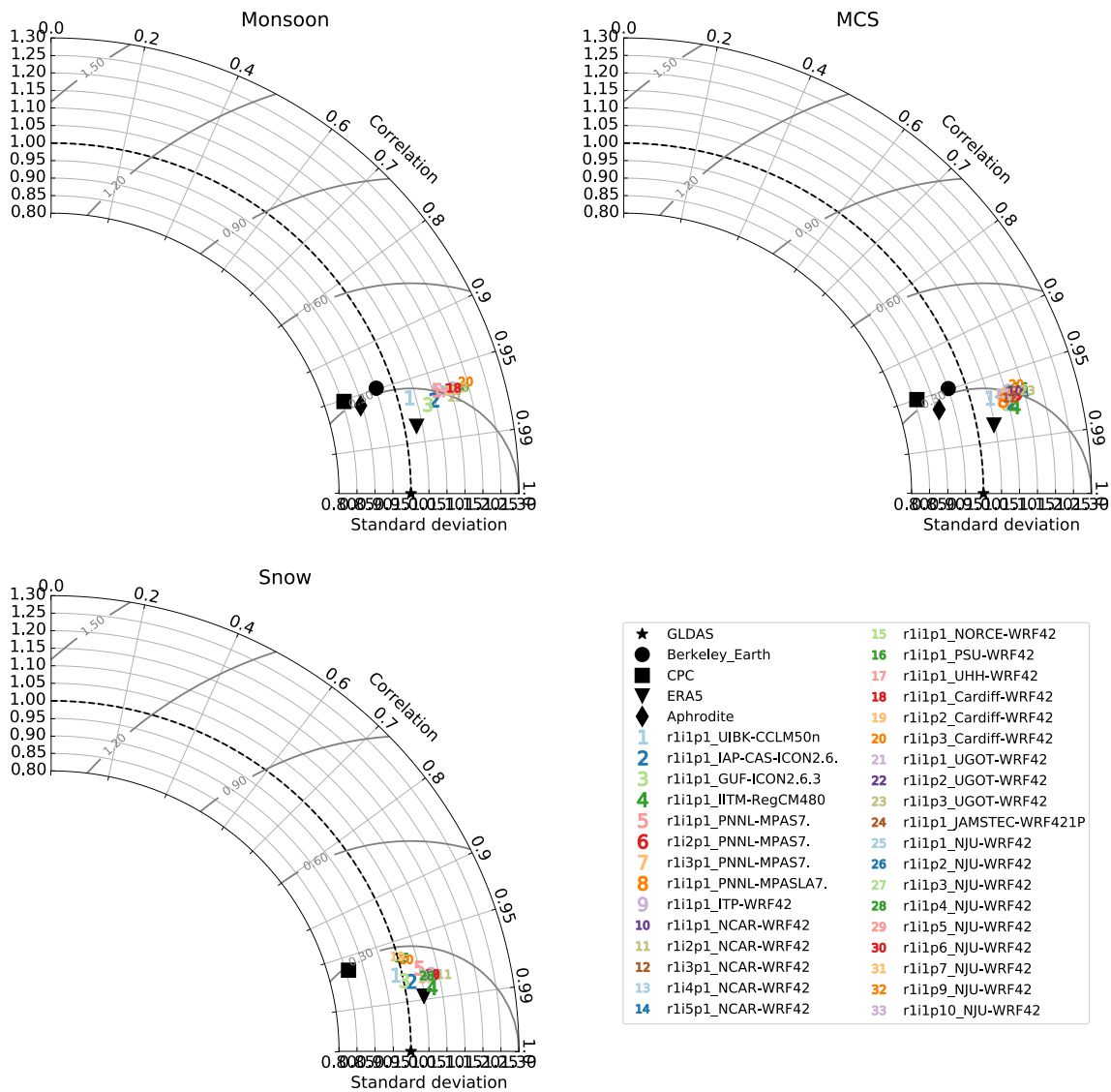


Fig. 11 Taylor diagrams showing the case average T2M pattern correlation, spatial standard deviation, and centred root mean square error comparing observational (black symbols) and modeled T2M (colored numbers) compared to GLDAS observations

high-performance computing (HPC) systems. These uncertainties are typically an order of magnitude smaller than the leading sources of uncertainty and do not affect our results substantially. Also, sensitivities to the use of a scale-aware deep convection scheme and different land surface models are small. However, land surface model sensitivities are likely underestimated in these short case study simulations since land surface processes can have a long memory, and uncertainties might grow in climate-length simulations.

The leading sources of WRF modeling uncertainties are the formulation of the microphysics, PBL schemes, and regional domain size. Which uncertainty source dominates is case- and metric-dependent. Small sensitivities are found for simulating spatial T2M patterns (Fig. 13c), except for varying the microphysics during the Snow case where the

WDM7 and WDM6 schemes result in lower correlation coefficients compared to the other tested schemes. Similarly, WDM7 and WDM6 result in larger T2M absolute biases (Fig. 13d). For precipitation metrics, microphysics uncertainties are largest for the Monsoon and MCS case and smallest for the Snow case. Again, the usage of the WDM6 and particularly the WDM7 scheme results in lower model performance concerning the simulation of precipitation patterns. Simulations that use the Thompson and Yin microphysics result in the overall best performance in capturing precipitation. Concerning PBL schemes, using the MYNN3 scheme results in sub-optimal performance for simulating T2M absolute differences, spatial patterns, and precipitation pattern correlations in all simulated cases. Using the YSU or Bourgeault PBL schemes provides the overall best

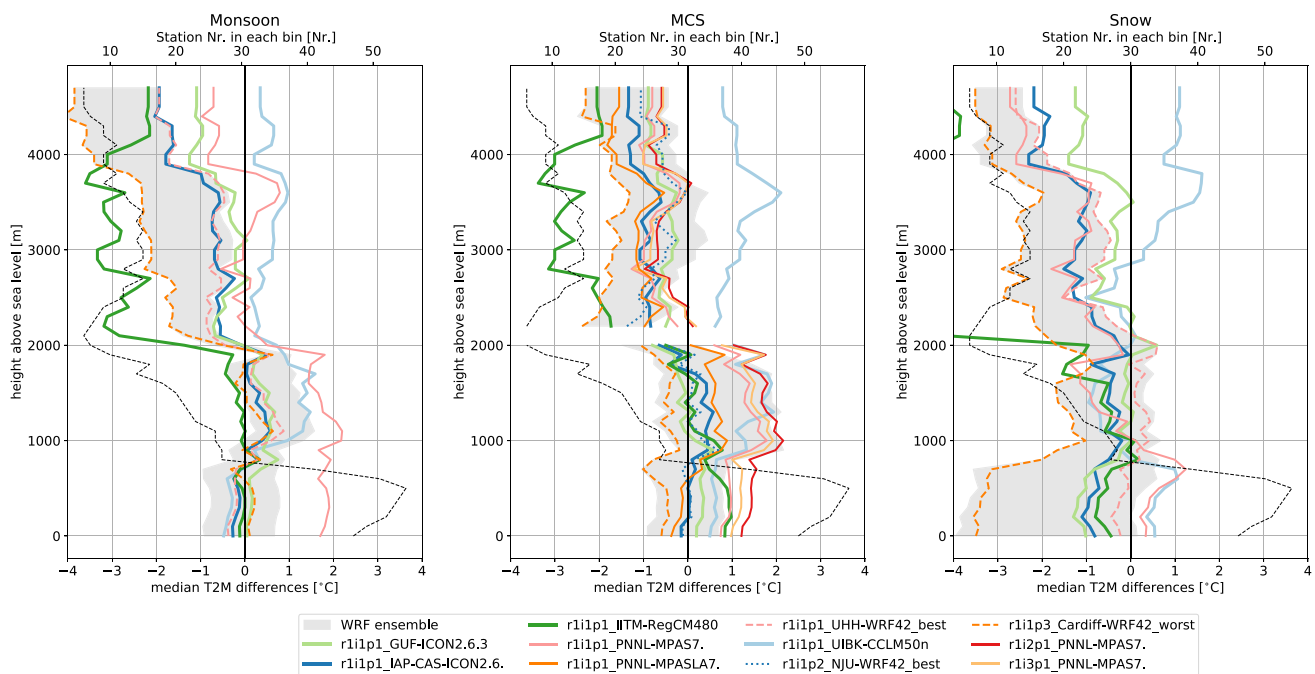


Fig. 12 Differences in T2M between model simulations and hourly HadISD station observations dependent on the height above sea level. The spatial station distribution is the same as shown in the maps in Fig. 10. Differences are calculated in bins with 100 m size and we use a ± 250 m window around each bin to reduce noise. The WRF ensemble spread is shown in gray contours and only the WRF simulations

with the lowest and largest absolute difference to the station data are shown. The r1i1p1_IITM-RegCM480 results are off the chart to the left and not visible in these plots. The number of stations in each bin is shown as a dotted black line on the secondary x-axis. We only show values for bins with more than five stations

performance concerning T2M metrics while schemes other than MYNN3 perform similarly well for precipitation metrics. Performing WRF simulations on the large domain (D2) always results in better T2M and precipitation simulations compared to simulations on D1. T2M improvements are particularly large during the Monsoon case, while absolute precipitation differences are not improved during this case.

4 Summary, discussion, and conclusions

In this paper, we present the first results of the Convection-Permitting Third Pole (CPTP) CORDEX Flagship Pilot Study, which is an internationally coordinated effort to improve our understanding of climate change impacts on the water cycle and its extremes over the TP region. We outline the experimental design and show results from multi-model, multi-physics case study simulations that focus on a flood-producing MCS case in 2008, a heavy rain-producing Monsoon period in 2014, and a heavy snow event in October 2018. The primary goal of these experiments is to better understand the performance of state-of-the-art, non-hydrostatic regional modeling systems in simulating precipitation and T2M during different weather situations over the TP region and to find suitable model settings that can be used

for climate-length runs in the future. The following points summarize our main findings:

- The performance of the five participating modeling systems is comparable but varies from case to case and among metrics. Overall, ICON and MPAS are performing best in simulating precipitation while RegCM4 performs best in simulating T2M.
- While there is no obvious connection between the KE spectra of a model and its skill in simulating precipitation and T2M, the spectra show important differences related to the model formulation and indicate that models like e.g. WRF, CCLM, and ICON are characterized by higher variability at smaller scales as compared to e.g. RegCM4.
- The large number of WRF simulations allows us to investigate sensitivities to model physics. The WRF multi-physics ensemble typically encompasses the spread of the other modeling systems for simulating precipitation, similar to previously published results over Europe Regional climate (2015). This is different for T2M, where changing the modeling system can substantially contribute to the spread of simulated results.
- Differences in observational datasets are the dominant source of uncertainty in the model evaluation and are typically larger than the model formulation, and model

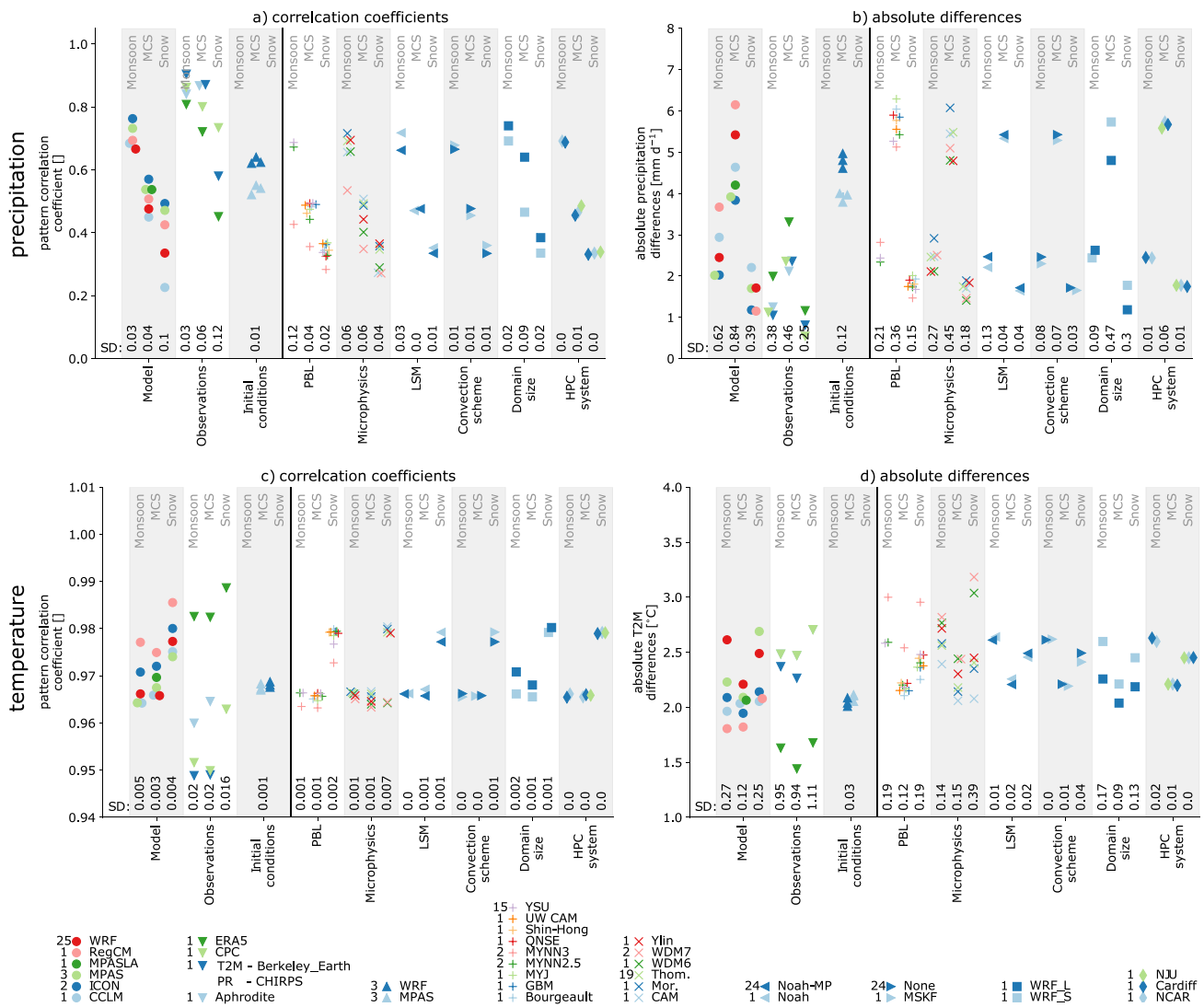


Fig. 13 Pattern correlation coefficients for event average precipitation (a) and T2M (c) and domain average absolute precipitation (b) and T2M differences (d). IMERG and GLDAS are used as reference for precipitation and T2M analyses respectively. Nine groups of points are shown for each case. The spread of these points provide an uncertainty estimate from a specified source: “Model” is the RCM formulation uncertainty, “Observation” represents the uncertainty between different observational products, “Initial Condition” is associated with the spread within two time-lagged initial condition ensembles (not available for the MCS case), “PBL” uncertainties associated

with different planetary boundary layer schemes in WRF, “Microphysics” formulation uncertainty in WRF, “LSM” show land surface model uncertainties in WRF, “Convective scheme” shows the impact of using a scale aware cumulus scheme or no convection scheme in WRF, “Domain size” shows sensitivities to the RCM domain size in WRF, and HPC system shows the spread in identical WRF simulations that were run on different computing systems. The standard deviation (SD) of each point cloud is shown at the bottom of each plot. The number of members in each averaged group is shown in the legend

physics uncertainties. Model biases and observational uncertainties are particularly large for the Snow case, which might be partly related to precipitation undercatch issues Prein and Gobiet (2017). This highlights a major challenge for evaluating model simulations in this region and observationally constraining the water and energy cycle over the TP. There is an urgent need to improve our in-situ and remotely sensed observational capabilities over the TP, which is one of the main goals of the Third

Pole Environment (TPE) Yao et al. (2012) and Asian Precipitation Experiment (AsiaPEX) Asian Precipitation Experiment (2022) projects. Studies have shown that kilometer-scale models can simulate snowfall very well in data rich regions (Ikeda et al. 2010, 2021) and can even outperform our observational capabilities in mountainous regions (Lundquist et al. 2019). Therefore, future efforts should focus on fusing high-quality observational and kilometer-scale model output (Crespi et al. 2019; T.L.

Table 1 Main model settings of reference experiments

Model	Ref-erence	LBC frequ.	Δx	Nesting	Buffer [cells]	levels	Radiation	Shallow Convection	Micro-physics	Land-surface	PBL	Soil initiali- zation	Aerosols	Lake model	Δt
WRF 4.2	Skamar- rock and Klemp (2008); Powers et al. (2017)	6-h	4 km	4 km is nested in 12 km parent run	4	38	RRTMG scheme for LW and SW Ruiz-Arias et al. (2013)	None	Thompson et al. (2008) Thomp- son et al. (2004)	Noah-MP Niu et al. (2011)	Yonsei University (YSU) Hong et al. (2006); Hong (2010)	Initialized with 1/2 year 12 km spinup simulation	None	Lake surface temperature is calculated from monthly mean 2 m air tem- perature	15 s
MPAS- Atm. 7.0	Skamarock et al. (2012)	Global VR mesh; Daily for SST/sea ice no	4 km over TP, 32 km over the rest of the globe	N.A.	N.A.	55	RRTMG scheme for LW and SW Iacono et al. (2008)	Scale-aware Grell-Freitas and Grell-Freitas (2014)	Thompson and Thompson et al. (2008)	Noah Chen and Dudhia (2001)	MYNN level 2.5 Nakanishi and Niino (2009)	From ERA5	None	None	24 s
MPAS- Atm. 7.0	Skamarock et al. (2018)	6-hour for lateral BC, and daily for SST/sea ice	4 km	ERA5	5	55	RRTMG scheme for LW and SW Iacono et al. (2008)	Scale-aware Grell-Freitas and Grell-Freitas (2014)	Thompson and Thompson et al. (2008)	Noah Chen and Dudhia (2001)	MYNN level 2.5 Nakanishi and Niino (2009)	From ERA5	None	None	12 s
RegCM 4.8.0	Giorgi et al. (2012); Coppola et al. (2021)	6-h	4 km	4 km simulation is forced with hourly ERA5	12	41	CCM3 Kiehl et al. (1996)	None	SUBgrid EXPLICIT moisture scheme (SUBEX) Pal et al. (2000)	Biosphere- Atmos- phere Transfer Scheme version 1e Dickinson (1993)	Holtlag non-local diffusion scheme Holtlag et al. (1990)	From ERA5	None	None	10 s
COSMO- CLM v.5.0.n1	Rockel et al. (2008); Baldauf et al. (2011); Fuhrer et al. (2014)	6-h	2.2 km	2.2 km simulation is nested in a 12 km parent domain	25	60	Ritter and Geleyn (1992) Ritter and Geleyn (1992) for short- and long-wave radiation	Tiedtke scheme for shal- low con- vection Tiedtke (1989)	One-moment scheme Doms and Schättler (2022); Seifert (2008)	TERRA (multi- layer version)	1-D TKE based diagnostic (level 2.5) closure	Soil and snow fields in the 2.2 km simu- lations are initialized from a 1-year spinup simula- tion with the 12-km domain	AeroCom Global AOD data	Flake Mironov (2005)	15 s

Table 1 (continued)

Model	Reference	LBC frequ.	Δx	Nesting	Buffer [cells]	levels	Radiation	Shallow Convection	Micro-physics	Land-surface	PBL	Soil initial-ization	Aerosols	Lake model	Δt
ICON 2.6.1	Zängl et al. (2015); Klocke et al. (2017)	3-h	3.3 km	ERA5	8	75	RRTM scheme Mlawer et al. (1997)	None	one-moment cloud microphysical scheme with graupel Baldauf et al. (2011)	Tiled TERRA Heise et al. (2006); Schulz et al. (2016)	Prognostic TKE Raschendorfer (2001)	From ERA5	None	Flake Mironov (2005)	30 s
ICON 2.6.3	Pham et al. (2021)	1-h	3.3 km	ERA5	10	50	RRTM scheme Mlawer et al. (1997)	Tiedtke–Bechtold Tiedtke (1989); Bechtold et al. (2004)	One-moment cloud microphysical scheme with graupel Baldauf et al. (2011)	Tiled TERRA Heise et al. (2006); Schulz et al. (2016)	Orr et al. (2010) Orr et al. (2010)	From ERA5	Tegen JGR 1997 (NASA/GISS) Tegen et al. (1997)	Flake Mironov (2005)	20 s

et al. [in press](#)) and use the latter to inform observational uncertainties Ouyang et al. (2021).

- WRF modeling experiments show that sensitivities due to the domain size (comparing simulations on D1 and D2) are of a similar order of magnitude as uncertainties stemming from the microphysics and PBL scheme. Generally, running the WRF kilometer-scale simulations on the large model domain (D2) improves the model results for all cases and metrics except for the Monsoon case absolute precipitation differences.
- WRF PBL scheme uncertainties have similar magnitudes for all cases and are comparable to uncertainties stemming from the microphysics. While the performance of a PBL scheme is case- and metric-dependent, we see that the MYNN3 scheme results in sub-optimal performance compared with the YSU, UW CAM, and MYNN2.5 schemes (except for absolute precipitation differences). However, the poorer performance of MYNN3 is largely due to its interactions with the WDM7 microphysics scheme while using it in combination with the Thompson scheme results in much better performance.
- Using the WDM6 and WDM7 microphysics schemes consistently results in lower than average performance independent of the case, variable, or metric in agreement to previous research over the Himalayas Orr et al. (2017). The other microphysics schemes perform equally well and have varying and non-systematic strengths and weaknesses depending on the case.
- There are systematic model deficiencies that most models share such as cold bias above 2000 m a.m.s.l. (except for CCLM) and a displacement of the heavy precipitation center towards the south (towards the north in case of RegCM) for the MCS case. Model performance in simulating precipitation is generally lowest during the Snow case, partly related to the large observational uncertainties. Future modeling efforts will aim to better understand the sources of these differences and to improve the overall model performance.

In-depth analyses that focus on single cases are ongoing that will provide additional insights into model performance (e.g., Kukilies et al. 93, for the MCS case). The results from this study will inform the modeling setup of climate time-scale simulations in the CPTP project. The CPTP WRF modeling community has already adapted their modeling strategy and will perform future simulations on the larger model domain (D2) due to the systematically better model performance when running simulations on D2 that is shown here. Currently, we are running ensemble simulations of the 2020 water year (Oct. 2019 to Sep. 2020) to better understand the seasonality of model biases and the potential for bias accumulations over time. We selected this recent period due to the availability of high-quality observational datasets

Table 2 Overview of WRF physics experiments

Name	YSU [108, 109] MYNN2.5 [114, 131, 132] MYJ [133, 134] MYNN3 [114, 131, 132] BouLac [135] QNSE, [136] UW CAM [137] Shin-Hong [138] GMB [139]	Noah-MP LSM ¹ [107] Noah LSM ¹ [140]	Thompson [112] WDM7 [141] WDM6 [142] Morrisson [143] Ylin [144] CAM [137]	No convection scheme MSKF ² [145, 146]	Domain D1 Domain D2 D1 direct ERA5 initialization -6h initialization -12h	Cases
	PBL schemes	LSM ¹	Microphysics	CS ⁴	Run Setup	
r1i1p1_NCAR						MoMCSn
r1i2p1_NCAR						MoMCSn
r1i3p1_NCAR						MC
r1i4p1_NCAR						MC
r1i5p1_NCAR						MC
r1i1p1_UGOT						MoMCSn
r1i1p2_UGOT						MoMCSn
r1i1p3_UGOT						MoMCSn
r1i1p1_JAMSTEC						MoMCSn
r1i1p1_UHH						MoMCSn
r1i1p1_Cardiff						MoMCSn
r1i1p2_Cardiff						MoMCSn
r1i1p3_Cardiff						MoMCSn
r1i1p1_ITP						MoMCSn
r1i1p1_PSU						MoMCSn
r1i1p1_NORCE						MoMCSn
r1i1p1_NJU						MCSn
r1i1p2_NJU						MoMCSn
r1i1p3_NJU						MCSn
r1i1p4_NJU						MCSn
r1i1p5_NJU						MCSn
r1i1p6_NJU						MCSn
r1i1p7_NJU						MCSn
r1i1p9_NJU						MCSn
r1i1p10_NJU						MCSn

¹Land surface model (LSM).

²Multi-scale Kain-Fritsch deep convection scheme.

³High performing computer (HPC).

⁴Cumulus Scheme (CS).

Gray cells show the reference physics setting while red cells indicate that the correspondent physics option has been changed compared to the reference setup. The rightmost column shows if the simulation has been performed for the Monsoon (Mo), MCS (MC), and Snow (Sn) case

over the TP from the TPE project Yao et al. (2012). These year-long simulations will be the basis for decadal runs of historical and future climate periods that will be performed by CPTP modelers in the next three years. Those runs will provide unprecedented insights into the changing energy and water cycle over the TP.

One key finding of this paper is the urgent need to better constrain water cycle processes over the TP region. This is essential not only for model validation but also to monitor climate and environmental changes in this vulnerable area. High-quality in-situ and remote sensing observations are essential for this task but are extremely challenging to

obtain due to the remoteness and extreme environments of the TP region. Fusing observational datasets with high-resolution modeling systems by creating e.g., a kilometer-scale regional reanalysis, such as has been done in other mountain regions Lussana et al. (2019), could alleviate some of the observational challenges and modeling biases and allow us to gain novel insights into the weather and climate of the TP.

Acknowledgements UIBK acknowledges PRACE for awarding them access to Piz Daint at the Swiss National Supercomputing Center (CSCS, Switzerland). They also acknowledge the Federal Office for Meteorology and Climatology MeteoSwiss, the Swiss National Supercomputing Centre (CSCS), and ETH Zürich for their contributions to

the development of the GPU-accelerated version of COSMO. In addition, they acknowledge DKRZ for providing COSMO-ready ERA5 boundary data. We would like to acknowledge high-performance computing support from Cheyenne (doi:10.5065/D6RX99HX) provided by NCAR's Computational and Information Systems Laboratory. The MPAS simulations were performed using computational resources provided by the National Energy Research Scientific Computing Center (NERSC), a DOE Office of Science User Facility supported by the Office of Science of the U.S. Department of Energy under Contract DE-AC02-05CH11231. K.S. and R.L. were supported by the U.S. Department of Energy Office of Science Biological and Environmental Research as part of the Global and Regional Model Analysis program area. S.S. acknowledges the Data Analyzer in JAMSTEC for the WRF simulations and is supported by JSPS KAKENHI Grant Number JP20K04095. The computations by the University of Gothenburg were enabled by resources provided by the Swedish National Infrastructure for Computing (SNIC) at the National Supercomputer Centre in Sweden (NSC) partially funded by the Swedish Research Council through grant agreement no. 2018-05973. XC acknowledges the high-performance computing support from the Texas Advanced Computing Center (TACC) and San Diego Supercomputer Center (SDSC). S.J. acknowledges the support provided for the RegCM4 simulations by the IITM Pratyush high performance computing facility. This is a contribution no 10 to CORDEX-FPS-CPTP.

Author Contributions All authors contributed to the study conception and design. The first draft of the manuscript was written by Andreas F. Prein and Nikolina Ban and all authors commented on previous versions of the manuscript. All authors read and approved the final manuscript.

Funding UHH is funded by the Deutsche Forschungsgemeinschaft (DFG, German Research Foundation) under Germany's Excellence Strategy—EXC 2037 'CLICCS—Climate, Climatic Change, and Society'—Project Number: 390683824, contribution to the Center for Earth System Research and Sustainability (CEN) of Universität Hamburg. PKP is funded by the Deutsche Forschungsgemeinschaft (DFG, German Research Foundation)—TRR 301—Project-ID 428312742. SS and LL gratefully acknowledge the support of a Bjerknes Fast Track Initiative from the Norwegian Education Directorate and HPC support through NOTUR/NorStore projects NN9820K/NS9001K. NCAR is sponsored by the National Science Foundation under Cooperative Agreement 1852977. PNNL is operated for the Department of Energy by Battelle Memorial Institute under contract DE-AC05-76RL01830. UGOT is supported by TPE via the Strategic Priority Research Program of the Chinese Academy of Sciences (XDA20060402) and Swedish MERGE. UHH also acknowledges the use of DKRZ resources granted by its Scientific Steering Committee under project ID numbers uc0977 & mh1212.

Data availability The datasets generated during and analysed during the current study are available from the corresponding author on reasonable request.

Declarations

Conflict of interest None.

Author Contributions Prof. BA was added as an author during the revisions of this paper. Prof. Ahrens contributed to the creation of the GUF-ICON2.3.6 simulations and supported the writing of this manuscript.

References

- Asian Precipitation Experiment (AsiaPEX). <http://iceds.cc.kagawa-u.ac.jp/asiapex/#:~:text=We%20just%20launched%20Asian%20Precipitation,Scientific%20Research%20and%20Prediction%20Initiative>. Accessed: 2022-04-10 (2022)
- Bae SY, Hong S-Y, Tao W-K (2019) Development of a single-moment cloud microphysics scheme with prognostic hail for the Weather Research and Forecasting (WRF) model. *Asia-Pacific J Atmos Sci* 55(2):233–245
- Baldauf M, Seifert A, Förstner J, Majewski D, Raschendorfer M, Reinhardt T (2011) Operational convective-scale numerical weather prediction with the COSMO model: description and sensitivities. *Mon Weather Rev* 139(12):3887–3905
- Ban N, Schmidli J, Schär C (2014) Evaluation of the convection-resolving regional climate modeling approach in decade-long simulations. *J Geophys Res Atmos* 119:7889–7907. <https://doi.org/10.1002/2014JD021478>
- Ban N, Schmidli J, Schar C (2015) Heavy precipitation in a changing climate: Does short-term summer precipitation increase faster? *Geophys Res Lett* 42(4):1165–1172. <https://doi.org/10.1002/2014GL062588>
- Ban N, Caillaud C, Coppola E, Pichelli E, Sobolowski S, Adinolfi M, Ahrens B, Alias A, Anders I, Bastin S et al (2021) The first multi-model ensemble of regional climate simulations at kilometer-scale resolution, part i: evaluation of precipitation. *Clim Dyn* 57:1–28. <https://doi.org/10.1007/s00382-021-05708-w>
- Barlage M, Chen F, Rasmussen R, Zhang Z, Miguez-Macho G (2021) The importance of scale-dependent groundwater processes in land-atmosphere interactions over the central United States. *Geophysical Research Letters* 48(5):2020–092171
- Bartsotas N, Anagnostou E, Nikolopoulos E, Kallos G (2018) Investigating satellite precipitation uncertainty over complex terrain. *J Geophys Res* 123(10):5346–5359
- Bechtold P, Chaboureaud J-P, Beljaars A, Betts A, Köhler M, Miller M, Redelsperger J-L (2004) The simulation of the diurnal cycle of convective precipitation over land in a global model. *Q J R Meteorol Soc* 130(604):3119–3137
- Beck HE, Wood EF, McVicar TR, Zambrano-Bigiarini M, Alvarez-Garreton C, Baez-Villanueva OM, Sheffield J, Karger DN (2020) Bias correction of global high-resolution precipitation climatologies using streamflow observations from 9372 catchments. *J Clim* 33(4):1299–1315
- Belušić A, Prtenjak MT, Gütler I, Ban N, Leutwyler D, Schär C (2018) Near-surface wind variability over the broader adriatic region: insights from an ensemble of regional climate models. *Clim Dyn* 50(11):4455–4480. <https://doi.org/10.1007/s00382-017-3885-5>
- Blažiča V, Žagar N, Strajnar B, Cedilnik J (2013) Rotational and divergent kinetic energy in the mesoscale model aladin. *Tellus A* 65(1):18918
- Bougeault P, Lacarrere P (1989) Parameterization of orography-induced turbulence in a mesobeta-scale model. *Mon Weather Rev* 117(8):1872–1890
- T.L., Y., Chan D., T., Piao, S (in press) Reflections and future strategies for the Third Pole Environment. *Nature Reviews Earth and Environment*
- Chen F, Dudhia J (2001) Coupling an advanced land surface-hydrology model with the Penn State-NCAR MM5 modeling system. Part I: Model implementation and sensitivity. *Mon Weather Rev* 129(4):569–585
- Clark P, Roberts N, Lean H, Ballard SP, Charlton-Perez C (2016) Convection-permitting models: a step-change in rainfall forecasting. *Meteorol Appl* 23(2):165–181
- Coppola E, Sobolowski S, Pichelli E, Raffaele F, Ahrens B, Anders I, Ban N, Bastin S, Belda M, Belusic D et al (2020) A

- first-of-its-kind multi-model convection permitting ensemble for investigating convective phenomena over Europe and the Mediterranean. *Clim Dyn* 55:3–34. <https://doi.org/10.1007/s00382-018-4521-8>
- Coppola E, Stocchi P, Pichelli E, Torres Alavez JA, Glazer R, Giuliani G, Di Sante F, Nogherotto R, Giorgi F (2021) Non-Hydrostatic RegCM4 (RegCM4-NH): model description and case studies over multiple domains. *Geosci Model Dev* 14(12):7705–7723
- Crespi A, Lussana C, Brunetti M, Dobler A, Maugeri M, Tveit OE (2019) High-resolution monthly precipitation climatologies over Norway (1981–2010): joining numerical model data sets and in situ observations. *Int J Climatol* 39(4):2057–2070
- Curio J, Schiemann R, Hodges KI, Turner AG (2019) Climatology of Tibetan plateau vortices in reanalysis data and a high-resolution global climate model. *J Clim* 32(6):1933–1950
- Dai Y, Chen D, Yao T, Wang L (2020) Large lakes over the Tibetan Plateau may boost snow downwind: implications for snow disaster. *Sci Bull* 65(20):1713–1717
- Denis B, Cote J, Laprise R (2002) Spectral decomposition of two-dimensional atmospheric fields on limited-area domains using the discrete cosine transform (dct). *Mon Weather Rev* 130(7):1812–1829
- Dickinson RE (1993) Biosphere atmosphere transfer scheme (BATS) version 1e as coupled to the NCAR community climate model. NCAR Tech. Note TH-387+ STR
- Doms G, Schättler U (2002) A description of the nonhydrostatic regional model LM. Part I: Dynamics and Numerics, Deutscher Wetterdienst, Offenbach 520
- Duda MG, Fowler LD, Skamarock WC, Roesch C, Jacobsen D, Ringler TD (2019) MPAS-Atmosphere Model User's Guide Version 7.0. Technical report, NCAR, Boulder, Colo
- Dunn RJ, Willett KM, Parker DE, Mitchell L (2016) Expanding Had-Isd: Quality-controlled, sub-daily station data from 1931. *Geosci Instrumentation Methods Data Syst* 5(2):473–491
- Eaton B (2011) User's guide to the community atmosphere model CAM-5.1. 1. NCAR
- Ek M, Mitchell K, Lin Y, Rogers E, Grunmann P, Koren V, Gayno G, Tarpley J (2003) Implementation of Noah land surface model advances in the National Centers for Environmental Prediction operational mesoscale Eta model. *J Geophys Res* 108(D22)
- Feng X, Liu C, Rasmussen R, Fan G (2014) A 10-yr climatology of Tibetan plateau vortices with NCEP climate forecast system reanalysis. *J Appl Meteorol Climatol* 53(1):34–46
- Fuhrer C, Oliver and Osuna, Lapillonne X, Gysi T, Cumming B, Bianco M, Arteaga A, Schulthess T (2014) Towards a performance portable, architecture agnostic implementation strategy for weather and climate models. *Supercomputing Frontiers and Innovations* 1:45–62
- Funk C, Peterson P, Landsfeld M, Pedreros D, Verdin J, Shukla S, Husak G, Rowland J, Harrison L, Hoell A et al (2015) The climate hazards infrared precipitation with stations—a new environmental record for monitoring extremes. *Sci Data* 2(1):1–21
- Giorgi F, Gutowski WJ Jr (2015) Regional dynamical downscaling and the CORDEX initiative. *Annual review of environment and resources* 40:467–490
- Giorgi F, Coppola E, Solmon F, Mariotti L, Sylla M, Bi X, Elguindi N, Diro G, Nair V, Giuliani G et al (2012) RegCM4: model description and preliminary tests over multiple CORDEX domains. *Climate Research* 52:7–29
- Glotfelty T, Alapaty K, He J, Hawbecker P, Song X, Zhang G (2019) The Weather Research and Forecasting Model with Aerosol-Cloud Interactions (WRF-ACI): Development, Evaluation, and Initial Application. *Mon Weather Rev* 147(5):1491–1511
- Grell GA, Freitas SR (2014) A scale and aerosol aware stochastic convective parameterization for weather and air quality modeling. *Atmos Chem Phys* 14(10):5233–5250
- Grenier H, Bretherton CS (2001) A moist PBL parameterization for large-scale models and its application to subtropical cloud-topped marine boundary layers. *Mon Weather Rev* 129(3):357–377
- Gutowski WJ Jr, Giorgi F, Timbal B, Frigon A, Jacob D, Kang H-S, Raghavan K, Lee B, Lennard C, Nikulin G et al (2016) WCRP coordinated regional downscaling experiment (CORDEX): a diagnostic MIP for CMIP6. *Geosci Model Dev* 9(11):4087–4095
- Hasson S, Saeed F, Böhner J, Schluessner C-F (2019) Water availability in Pakistan from Hindukush-Karakoram-Himalayan watersheds at 1.5 C and 2 C Paris Agreement targets. *Adv Water Resources* 131:103365
- Hasson S, Böhner J, Chishtie F (2016) Low Fidelity of Present-day Climate Modelling experiments and future climatic uncertainty over Himalayan watersheds of Indus basin. *Clim. Dyn*
- Heise E, Ritter B, Schrodin R, Wetterdienst D (2006) Operational Implementation of the Multilayer Soil Model. Citeseer, ???
- Hentgen L, Ban N, Kroner N, Leutwyler D, Schar C (2019) Clouds in convection-resolving climate simulations over Europe. *J Geophys Res* 124(7):3849–3870. <https://doi.org/10.1029/2018JD030150>
- Hersbach H, Bell B, Berrisford P, Hirahara S, Horányi A, Muñoz-Sabater J, Nicolas J, Peubey C, Radu R, Schepers D et al (2020) The ERA5 global reanalysis. *Q J R Meteorol Soc* 146(730):1999–2049
- Holtstlag A, De Bruijn E, Pan H (1990) A high resolution air mass transformation model for short-range weather forecasting. *Mon Weather Rev* 118(8):1561–1575
- Hong S-Y (2010) A new stable boundary-layer mixing scheme and its impact on the simulated East Asian summer monsoon. *Quarterly Journal of the Royal Meteorological Society* 136(651):1481–1496
- Hong S-Y, Noh Y, Dudhia J (2006) A new vertical diffusion package with an explicit treatment of entrainment processes. *Mon Weather Rev* 134(9):2318–2341
- Huffman G (2019) IMERG V06 quality index. https://gpm.nasa.gov/sites/default/files/2020-02/IMERGV06_QI_0.pdf
- Huffman GJ, Bolvin DT, Braithwaite D, Hsu K, Joyce R, Xie P, Yoo S-H (2015) NASA global precipitation measurement (GPM) integrated multi-satellite retrievals for GPM (IMERG). Algorithm Theoretical Basis Document (ATBD) Version 4:26
- Iacono MJ, Delamere JS, Mlawer EJ, Shephard MW, Clough SA, Collins WD (2008) Radiative forcing by long-lived greenhouse gases: Calculations with the AER radiative transfer models. *J Geophys Res* 113(D13)
- Ikeda K, Rasmussen R, Liu C, Gochis D, Yates D, Chen F, Tewari M, Barlage M, Dudhia J, Miller K, Arsenault K, Grubišić V, Thompson G, Guttman E (2010) Simulation of seasonal snowfall over Colorado. *Atmos Res* 97(4):462–477. <https://doi.org/10.1016/j.atmosres.2010.04.010>
- Ikeda K, Rasmussen R, Liu C, Gochis D, Yates D, Chen F, Tewari M, Barlage M, Dudhia J, Miller K et al (2010) Simulation of seasonal snowfall over Colorado. *Atmos Res* 97(4):462–477
- Ikeda K, Rasmussen R, Liu C, Newman A, Chen F, Barlage M, Guttman E, Dudhia J, Dai A, Luce C et al (2021) Snowfall and snowpack in the Western US as captured by convection permitting climate simulations: current climate and pseudo global warming future climate. *Clim Dyn* 57(7):2191–2215
- Janjić ZI (1994) The step-mountain eta coordinate model: Further developments of the convection, viscous sublayer, and turbulence closure schemes. *Monthly weather review* 122(5):927–945
- Ju L, Ringler T, Gunzburger M (2011) Voronoi tessellations and their application to climate and global modeling. In: *Numerical Techniques for Global Atmospheric Models*, pp. 313–342. Springer, ???
- Karki R, Hasson S, Gerlitz L, Schickhoff U, Scholten T, Böhner J (2017) Quantifying the added value of high resolution climate

- models: a systematic comparison of WRF simulations for complex Himalayan terrain. *Earth Syst Dyn* 8:507–528
- Karki R, Hasson S, Gerlitz L, Talchabhadel R, Schenk E, Schickhoff U, Scholten T, Böhner J (2018) Wrf-based simulation of an extreme precipitation event over the central himalayas: atmospheric mechanisms and their representation by microphysics parameterization schemes. *Atmosph Res* 214:21–35
- Karki R, Hasson S.u, Schickhoff U, Scholten T, Böhner J, Gerlitz L (2020) Near surface air temperature lapse rates over complex terrain: a WRF based analysis of controlling factors and processes for the central Himalayas. *Clim Dyn* 54(1):329–349
- Kendon EJ, Fosser G, Murphy J, Chan S, Clark R, Harris G, Lock A, Lowe J, Martin G, Pirret J, Roberts N, Sanderson M, Tucker S (2019) UKCP Convection-permitting model projections: Science report. UK Met Office
- Kendon EJ, Roberts NM, Senior CA, Roberts MJ (2012) Realism of Rainfall in a Very High-Resolution Regional Climate Model. *J Clim* 25(17):5791–5806. <https://doi.org/10.1175/JCLI-D-11-00562.1>
- Kendon EJ, Roberts NM, Fowler HJ, Roberts MJ, Chan SC, Senior CA (2014) Heavier summer downpours with climate change revealed by weather forecast resolution model. *Nat Clim Change* 4:570–576. <https://doi.org/10.1038/nclimate2258>
- Kendon EJ, Stratton RA, Tucker S, Marsham JH, Berthou S, Rowell DP, Senior CA (2019) Enhanced future changes in wet and dry extremes over Africa at convection-permitting scale. *Nat Commun* 10:1794. <https://doi.org/10.1038/s41467-019-09776-9>
- Kiehl J, Hack J, Bonan G, Boville B, Briegleb B (1996) Description of the NCAR community climate model (CCM3). Technical Note. Technical report, National Center for Atmospheric Research, Boulder, CO (United States)
- Klemp JB (2011) A terrain-following coordinate with smoothed coordinate surfaces. *Mon Weather Rev* 139(7):2163–2169
- Klocke D, Brueck M, Hohenegger C, Stevens B (2017) Rediscovery of the doldrums in storm-resolving simulations over the tropical Atlantic. *Nat Geosci* 10(12):891–896
- Kotlarski S, Keuler K, Christensen OB, Colette A, Déqué M, Gobiet A, Goergen K, Jacob D, Lüthi D, van Meijgaard E, Nikulin G, Schä C, Teichmann C, Vautard R, Warrach-Sagi K, Wulfmeyer V (2014) Regional climate modeling on European scales: a joint standard evaluation of the EURO-CORDEX RCM ensemble. *Geosci Model Dev Discuss* 7:217–293. <https://doi.org/10.5194/gmdd-7-217-2014>
- Kukilies J, Prein AF, Curio J, Deliang C, Evaluating kilometer-scale multi-model and multi-physics ensemble simulations of a mesoscale convective system in the lee of the Tibetan Plateau. *J Clim* (In Review)
- Kukulies J, Chen D, Curio J (2021) The role of mesoscale convective systems in precipitation in the tibetan plateau region. *J Geophys Res* 126(23):2021–035279
- Li P, Furtado K, Zhou T, Chen H, Li J (2021) Convection-permitting modelling improves simulated precipitation over the central and eastern tibetan plateau. *Q J R Meteorol Soc* 147(734):341–362
- Lim K-SS, Hong S-Y (2010) Development of an effective double-moment cloud microphysics scheme with prognostic cloud condensation nuclei (CCN) for weather and climate models. *Mon Weather Rev* 138(5):1587–1612
- Lin C, Chen D, Yang K, Ou T (2018) Impact of model resolution on simulating the water vapor transport through the central Himalayas: implication for models' wet bias over the Tibetan Plateau. *Climate dynamics* 51(9):3195–3207
- Liu C, Ikeda K, Rasmussen R, Barlage M, Newman AJ, Prein AF, Chen F, Chen L, Clark M, Dai A, Dudhia J, Eidhammer T, Gochis D, Gutmann E, Kurkute S, Li Y, Thompson G, Yates D (2017) Continental-scale convection-permitting modeling of the current and future climate of North America. *Clim Dyn* 49(1):71–95. <https://doi.org/10.1007/s00382-016-3327-9>
- Lu X, Tang G, Wang X, Liu Y, Jia L, Xie G, Li S, Zhang Y (2019) Correcting GPM IMERG precipitation data over the Tianshan Mountains in China. *J Hydrol* 575:1239–1252
- Lundquist J, Hughes M, Gutmann E, Kapnick S (2019) Our skill in modeling mountain rain and snow is bypassing the skill of our observational networks. *Bull Am Meteorol Soc* 100(12):2473–2490
- Lussana C, Tveito OE, Dobler A, Tunheim K (2019) seNorge_2018, daily precipitation, and temperature datasets over Norway. *Earth System Science Data* 11(4):1531–1551
- Lüthi S, Ban N, Kotlarski S, Steger CR, Jonas T, Schär C (2019) Projections of alpine snow-cover in a high-resolution climate simulation. *Atmosphere* 10(8):463. <https://doi.org/10.3390/atmos10080463>
- Matte D, Laprise R, Thériault JM, Lucas-Picher P (2017) Spatial spin-up of fine scales in a regional climate model simulation driven by low-resolution boundary conditions. *Clim Dyn* 49(1):563–574
- Maussion F, Scherer D, Mölg T, Collier E, Curio J, Finkelnburg R (2014) Precipitation seasonality and variability over the tibetan plateau as resolved by the high asia reanalysis. *J Clim* 27(5):1910–1927. <https://doi.org/10.1175/JCLI-D-13-00282.1>
- Mesinger F (1993) Forecasting upper tropospheric turbulence within the framework of the Mellor-Yamada 2.5 closure. *Res. Activ. Atmos. Oceanic Mod*
- Mironov DV (2005) Parameterization of lakes in numerical weather prediction. Part 1: Description of a lake model. German Weather Service, Offenbach am Main, Germany
- Mlawer EJ, Taubman SJ, Brown PD, Iacono MJ, Clough SA (1997) Radiative transfer for inhomogeneous atmospheres: RRTM, a validated correlated-k model for the longwave. *J Geophys Res* 102(D14):16663–16682
- Mooney P, Broderick C, Bruyère C, Mulligan F, Prein A (2017) Clustering of observed diurnal cycles of precipitation over the United States for evaluation of a WRF multiphysics regional climate ensemble. *Journal of Climate* 30(22):9267–9286
- Morrison H, Thompson G, Tatarskii V (2009) Impact of cloud microphysics on the development of trailing stratiform precipitation in a simulated squall line: Comparison of one-and two-moment schemes. *Mon Weather Rev* 137(3):991–1007
- Nakanishi M, Niino H (2004) An improved Mellor-Yamada level-3 model with condensation physics: Its design and verification. *Boundary-layer Meteorol* 112(1):1–31
- Nakanishi M, Niino H (2009) Development of an improved turbulence closure model for the atmospheric boundary layer. *J Meteorol Soc Jpn Ser II* 87(5):895–912
- Nastrom G, Gage KS, Jaspersen W (1984) Kinetic energy spectrum of large-and mesoscale atmospheric processes. *Nature* 310(5972):36–38
- Niu G-Y, Yang Z-L, Mitchell KE, Chen F, Ek MB, Barlage M, Kumar A, Manning K, Niyogi D, Rosero E, et al (2011) The community Noah land surface model with multiparameterization options (Noah-MP): 1. Model description and evaluation with local-scale measurements. *Journal of Geophysical Research: Atmospheres* 116(D12)
- Olson JB, Kenyon JS, Angevine W, Brown JM, Pagowski M, Sušelj K, et al (2019) A description of the MYNN-EDMF scheme and the coupling to other components in WRF-ARW
- Orr A, Bechtold P, Scinocca J, Ern M, Janiskova M (2010) Improved middle atmosphere climate and forecasts in the ECMWF model through a nonorographic gravity wave drag parameterization. *J Clim* 23(22):5905–5926
- Orr A, Listowski C, Coustet M, Collier E, Immerzeel W, Deb P, Bannister D (2017) Sensitivity of simulated summer monsoonal

- precipitation in Langtang Valley, Himalaya, to cloud microphysics schemes in WRF. *J Geophys Res* 122(12):6298–6318
- Ouyang L, Lu H, Yang K, Leung LR, Wang Y, Zhao L, Zhou X, Chen Y, Jiang Y, Yao X (2021) Characterizing Uncertainties in Ground “Truth” of Precipitation Over Complex Terrain Through High-Resolution Numerical Modeling. *Geophys Res Lett* 48(10):2020–091950
- Pal JS, Small EE, Eltahir EA (2000) Simulation of regional-scale water and energy budgets: Representation of subgrid cloud and precipitation processes within RegCM. *J Geophys Res Atmosp* 105(D24):29579–29594
- Park S-H, Klemp JB, Skamarock WC (2014) A comparison of mesh refinement in the global MPAS-A and WRF models using an idealized normal-mode baroclinic wave simulation. *Mon Weather Rev* 142(10):3614–3634
- Pham TV, Steger C, Rockel B, Keuler K, Kirchner I, Mertens M, Rieger D, Zängl G, Früh B (2021) ICON in Climate Limited-area Mode (ICON release version 2.6. 1): a new regional climate model. *Geoscientific Model Development* 14(2):985–1005
- Pichelli E, Coppola E, Sobolowski S, Ban N, Giorgi F, Stocchi P, Alias A, Belušić D, Berthou S, Caillaud C et al (2021) The first multi-model ensemble of regional climate simulations at kilometer-scale resolution part 2: historical and future simulations of precipitation. *Clim Dyn* 56(11):3581–3602
- Plumb RA (1985) On the three-dimensional propagation of stationary waves. *J Atmos Sci* 42(3):217–229
- Pörtner H-O, Roberts DC, Masson-Delmotte V, Zhai P, Tignor M, Poloczanska E, Weyer N (2019) The ocean and cryosphere in a changing climate. IPCC Special Report on the Ocean and Cryosphere in a Changing Climate
- Powers JG, Klemp JB, Skamarock WC, Davis CA, Dudhia J, Gill DO, Coen JL, Gochis DJ, Ahmadov R, Peckham SE et al (2017) The weather research and forecasting model: overview, system efforts, and future directions. *Bull Am Meteorol Soc* 98(8):1717–1737
- Prein AF, Gobiet A (2017) Impacts of uncertainties in European gridded precipitation observations on regional climate analysis. *International Journal of Climatology* 37(1):305–327
- Prein AF, Gobiet A, Suklitsch M, Truhetz H, Awan NK, Keuler K, Georgievski G (2013) Added value of convection permitting seasonal simulations. *Climate Dyn* 41(9–10):2655–2677. <https://doi.org/10.1007/s00382-013-1744-6>
- Prein AF, Langhans W, Fossier G, Ferrone A, Ban N, Goergen K, Keller M, Tölle M, Gutjahr O, Feser F, Brisson E, Kollet S, Schmidli J, van Lipzig NPM, Leung R (2015) A review on regional convection-permitting climate modeling: demonstrations, prospects, and challenges. *Rev Geophys* 53(2):323–361. <https://doi.org/10.1002/2014RG000475>
- Prein AF, Langhans W, Fossier G, Ferrone A, Ban N, Goergen K, Keller M, Tölle M, Gutjahr O, Feser F, Brisson E, Kollet S, Schmidli J, van Lipzig NPM, Leung R (2015) A review on regional convection-permitting climate modeling: demonstrations, prospects, and challenges. *Rev Geophys* 53(2):323–361. <https://doi.org/10.1002/2014RG000475>
- Prein A, Rasmussen R, Wang D, Giangrande S (2021) Sensitivity of organized convective storms to model grid spacing in current and future climates. *Philosophical Trans R Soc A* 379(2195):20190546
- Prein A, Gobiet A, Truhetz H, Keuler K, Goergen K, Teichmann C, Fox Maule C, Van Meijgaard E, Déqué M, Nikulin G, et al (2016) Precipitation in the EURO-CORDEX 0.11deg and 0.44deg simulations: high resolution, high benefits? *Climate dynamics* 46(1):383–412
- Raschendorfer M (2001) The new turbulence parameterization of LM. *COSMO Newsletter* 1:89–97
- Rasmussen R, Liu C, Ikeda K, Gochis D, Yates D, Chen F, Tewari M, Barlage M, Dudhia J, Yu W et al (2011) High-resolution coupled climate runoff simulations of seasonal snowfall over Colorado: A process study of current and warmer climate. *Journal of Climate* 24(12):3015–3048
- Rasmussen R, Liu C, Ikeda K, Gochis D, Yates D, Chen F, Tewari M, Barlage M, Dudhia J, Yu W, Miller K, Arsenault K, Grubišić V, Thompson G, Gutmann E (2011) High-resolution coupled climate runoff simulations of seasonal snowfall over Colorado: a process study of current and warmer climate. *J Clim* 24:3015–3048. <https://doi.org/10.1175/2010JCLI3985.1>
- Rasmussen R, Ikeda K, Liu C, Gochis D, Clark M, Dai A, Gutmann E, Dudhia J, Chen F, Barlage M et al (2014) Climate change impacts on the water balance of the Colorado headwaters: high-resolution regional climate model simulations. *J Hydrometeorol* 15(3):1091–1116
- Rasmussen R, Ikeda K, Liu C, Gochis D, Clark M, Dai A, Gutmann E, Dudhia J, Chen F, Barlage M, Yates D, Zhang G (2014) Climate change impacts on the water balance of the Colorado headwaters: High-resolution regional climate model simulations. *Journal of Hydrometeorology* 15(3):1091–1116. <https://doi.org/10.1175/JHM-D-13-0118.1>
- Regional climate hindcast simulations within EURO-CORDEX (2015) evaluation of a WRF multi-physics ensemble, author=Katragkou, Eleni and García-Díez, Markel and Vautard, Robert and Sobolowski, S and Zanis, Prodromos and Alexandri, G and Cardoso, Rita M and Colette, Augustin and Fernandez, J and Gobiet, A and others. *Geoscientific model development* 8(3):603–618
- Ringler TD, Thuburn J, Klemp JB, Skamarock WC (2010) A unified approach to energy conservation and potential vorticity dynamics for arbitrarily-structured C-grids. *J Comput Phys* 229(9):3065–3090
- Ringler T, Petersen M, Higdon RL, Jacobsen D, Jones PW, Maltrud M (2013) A multi-resolution approach to global ocean modeling. *Ocean Modell* 69:211–232
- Ritter B, Geleyn J-F (1992) A comprehensive radiation scheme for numerical weather prediction models with potential applications in climate simulations. *Mon Weather Rev* 120(2):303–325
- Rockel B, Will A, Hense A (2008) The regional climate model COSMO-CLM (CCLM). *Meteorologische Zeitschrift* 17(4):347–348
- Rodell M, Houser P, Jambor U, Gottschalck J, Mitchell K, Meng C-J, Arsenault K, Cosgrove B, Radakovich J, Bosilovich M et al (2004) The global land data assimilation system. *Bull Am Meteorol Soc* 85(3):381–394
- Rohde R, Muller R, Jacobsen R, Perlmutter S, Rosenfeld A, Wurtele J, Curry J, Wickham C, Mosher S (2013) Berkeley Earth temperature averaging process. *Geoinformatics & Geostatistics* 1(2):1–13
- Rowell DP (2006) A demonstration of the uncertainty in projections of UK climate change resulting from regional model formulation. *Climatic Change* 79(3):243–257
- Ruiz-Arias JA, Dudhia J, Santos-Alamillos FJ, Pozo-Vázquez D (2013) Surface clear-sky shortwave radiative closure inter-comparisons in the Weather Research and Forecasting model. *J Geophys Res* 118(17):9901–9913
- Sanjay J, Krishnan R, Shrestha AB, Rajbhandari R, Ren G-Y (2017) Downscaled climate change projections for the Hindu Kush Himalayan region using CORDEX South Asia regional climate models. *Adv Clim Change Res* 8(3):185–198
- Schulz J-P, Vogel G, Becker C, Kothe S, Ahrens B (2016) Evaluation of the ground heat flux simulated by a multi-layer land surface scheme using high-quality observations at grass land and bare soil. *Meteor. Z.* 25(5):607–620. <https://doi.org/10.1127/metz/2016/0537>

- Seifert A (2008) On the parameterization of evaporation of raindrops as simulated by a one-dimensional rainshaft model. *J Atmosf Sci* 65(11):3608–3619
- Sharma S, Chen Y, Zhou X, Yang K, Li X, Niu X, Hu X, Khadka N (2020) Evaluation of GPM-Era satellite precipitation products on the southern slopes of the Central Himalayas against rain gauge data. *Remote Sens* 12(11):1836
- Shin HH, Hong S-Y (2015) Representation of the subgrid-scale turbulent transport in convective boundary layers at gray-zone resolutions. *Monthly Weather Review* 143(1):250–271
- Singh P, Kumar N (1997) Effect of orography on precipitation in the western Himalayan region. *J Hydrol* 199(1–2):183–206
- Skamarock WC (2004) Evaluating mesoscale NWP models using kinetic energy spectra. *Mon Weather Rev* 132(12):3019–3032
- Skamarock WC, Klemp JB (2008) A time-split nonhydrostatic atmospheric model for weather research and forecasting applications. *J Comput Phys* 227(7):3465–3485
- Skamarock WC, Klemp JB, Duda MG, Fowler LD, Park S-H, Ringler TD (2012) A multiscale nonhydrostatic atmospheric model using centroidal Voronoi tessellations and C-grid staggering. *Monthly Weather Review* 140(9):3090–3105
- Skamarock WC, Park S-H, Klemp JB, Snyder C (2014) Atmospheric kinetic energy spectra from global high-resolution nonhydrostatic simulations. *J Atmosf Sci* 71(11):4369–4381
- Skamarock WC, Duda MG, Ha S, Park S-H (2018) Limited-area atmospheric modeling using an unstructured mesh. *Mon Weather Rev* 146(10):3445–3460
- Sugimoto S, Ueno K, Fujinami H, Nasuno T, Sato T, Takahashi HG (2021) Cloud-resolving-model simulations of nocturnal precipitation over the Himalayan slopes and foothills. *J Hydrometeorol* 22(12):3171–3188
- Sugimoto S, Ueno K (2010) Formation of mesoscale convective systems over the eastern tibetan plateau affected by plateau-scale heating contrasts. *Journal of Geophysical Research: Atmospheres* 115(D16)
- Tang G, Clark MP, Papalexioiu SM, Ma Z, Hong Y (2020) Have satellite precipitation products improved over last two decades? A comprehensive comparison of GPM IMERG with nine satellite and reanalysis datasets. *Remote sensing of environment* 240:111697
- Tastula E-M, Galperin B, Dudhia J, LeMone MA, Sukoriansky S, Vihma T (2015) Methodical assessment of the differences between the QNSE and MYJ PBL schemes for stable conditions. *Q J R Meteorol Soc* 141(691):2077–2089
- Taylor KE (2001) Summarizing multiple aspects of model performance in a single diagram. *J Geophys Res* 106(D7):7183–7192
- Tegen I, Hollrig P, Chin M, Fung I, Jacob D, Penner J (1997) Contribution of different aerosol species to the global aerosol extinction optical thickness: Estimates from model results. *Journal of Geophysical Research: Atmospheres* 102(D20):23895–23915
- Thompson G, Rasmussen RM, Manning K (2004) Explicit forecasts of winter precipitation using an improved bulk microphysics scheme. Part I: description and sensitivity analysis. *Mon Weather Rev* 132(2):519–542
- Thompson G, Field PR, Rasmussen RM, Hall WD (2008) Explicit forecasts of winter precipitation using an improved bulk microphysics scheme. Part II: implementation of a new snow parameterization. *Mon Weather Rev* 136(12):5095–5115
- Tiedtke M (1989) A comprehensive mass flux scheme for cumulus parameterization in large-scale models. *Mon Weather Rev* 117(8):1779–1800
- Torma C, Giorgi F, Coppola E (2015) Added value of regional climate modeling over areas characterized by complex terrain-precipitation over the alps. *Journal of Geophysical Research: Atmospheres* 120(9), 3957–3972. <https://agupubs.onlinelibrary.wiley.com/doi/pdf/10.1002/2014JD022781>. 10.1002/2014JD022781
- Wang X, Chen D, Pang G, Anwar SA, Ou T, Yang M (2021) Effects of cumulus parameterization and land-surface hydrology schemes on Tibetan Plateau climate simulation during the wet season: Insights from the RegCM4 model. *Climate Dynamics* 57(7):1853–1879
- Xie P, Chen M, Shi W (2010) CPC unified gauge-based analysis of global daily precipitation. In: *Preprints, 24th Conf. on Hydrology, Atlanta, GA, Amer. Meteor. Soc, vol. 2*
- Yao T, Thompson LG, Mosbrugger V, Zhang F, Ma Y, Luo T, Xu B, Yang X, Joswiak DR, Wang W et al (2012) Third pole environment (TPE). *Environ Dev* 3:52–64
- Yatagai A, Kamiguchi K, Arakawa O, Hamada A, Yasutomi N, Kito A (2012) APHRODITE: constructing a long-term daily gridded precipitation dataset for Asia based on a dense network of rain gauges. *Bull Am Meteorol Soc* 93(9):1401–1415
- Zängl G, Reinert D, Rípodas P, Baldauf M (2015) The ICON (ICOSahedral Non-hydrostatic) modelling framework of DWD and MPI-M: Description of the non-hydrostatic dynamical core. *Q J R Meteorol Soc* 141(687):563–579
- Zeman C, Wedi NP, Dueben PD, Ban N, Schär C (2021) Model inter-comparison of cosmo 5.0 and ifs 45r1 at kilometer-scale grid spacing. *Geoscientific Model Development* 14(7):4617–4639
- Zhang F, Thapa S, Immerzeel W, Zhang H, Lutz A (2019) Water availability on the Third Pole: A review. *Water Security* 7:100033
- Zhao X, Lin Y, Luo Y, Qian Q, Liu X, Liu X, Colle BA (2021) A Double-Moment SBU-YLIN Cloud Microphysics Scheme and Its Impact on a Squall Line Simulation. *J Adv Model Earth Syst* 13(11):2021–002545
- Zheng Y, Alapaty K, Herwehe JA, Del Genio AD, Niyogi D (2016) Improving high-resolution weather forecasts using the Weather Research and Forecasting (WRF) Model with an updated Kain-Fritsch scheme. *Mon Weather Rev* 144(3):833–860

Publisher's Note Springer Nature remains neutral with regard to jurisdictional claims in published maps and institutional affiliations.

Springer Nature or its licensor (e.g. a society or other partner) holds exclusive rights to this article under a publishing agreement with the author(s) or other rightsholder(s); author self-archiving of the accepted manuscript version of this article is solely governed by the terms of such publishing agreement and applicable law.

Authors and Affiliations

Andreas F. Prein¹  · Nikolina Ban² · Tinghai Ou⁷ · Jianping Tang¹¹ · Koichi Sakaguchi³ · Emily Collier² · Sanjay Jayanarayanan⁴ · Lu Li⁵ · Stefan Sobolowski⁵ · Xingchao Chen⁶ · Xu Zhou⁸ · Hui-Wen Lai⁷ · Shiori Sugimoto⁹ · Liwei Zou¹² · Shabeh ul Hasson¹³ · Marie Ekstrom¹⁴ · Praveen Kumar Pothapakula^{16,17} · Bodo Ahrens¹⁶ · Romilly Stuart^{15,18} · Hans Christian Steen-Larsen¹⁵ · Ruby Leung³ · Danijel Belusic^{10,19} · Julia Kukulies⁷ · Julia Curio⁷ · Deliang Chen⁷

Nikolina Ban
nikolina.ban@uibk.ac.at

Tinghai Ou
tinghai.ou@gu.se

Jianping Tang
jptang@nju.edu.cn

Koichi Sakaguchi
Koichi.Sakaguchi@pnnl.gov

Emily Collier
emily.collier@uibk.ac.at

Sanjay Jayanarayanan
sanjay@tropmet.res.in

Lu Li
luli@norceresearch.no

Stefan Sobolowski
stso@norceresearch.no

Xingchao Chen
xzc55@psu.edu

Xu Zhou
xuzhou@itpcas.ac.cn

Hui-Wen Lai
hui-wen.lai@gu.se

Shiori Sugimoto
shiorisug@jamstec.go.jp

Liwei Zou
zoulw@lasg.iap.ac.cn

Shabeh ul Hasson
shabeh.hasson@uni-hamburg.de

Marie Ekstrom
mce7212@gmail.com

Praveen Kumar Pothapakula
praveen.pothapakula@kit.edu

Bodo Ahrens
Bodo.Ahrens@iau.uni-frankfurt.de

Romilly Stuart
romilly.harris-stuart@lscce.ipsl.fr

Hans Christian Steen-Larsen
Hans.Christian.Steen-Larsen@uib.no

Ruby Leung
ruby.leung@pnnl.gov

Danijel Belusic
danijel.belusic@smhi.se

Julia Kukulies
julia.kukulies@gu.se

Julia Curio
j.curio@reading.ac.uk

Deliang Chen
deliang@gvc.gu.se

² Department of Atmospheric and Cryospheric Sciences, University of Innsbruck, Innrain 52f, Innsbruck 6020, Tirol, Austria

³ Pacific Northwest National Laboratory, 902 Battelle Blvd, Richland, WA 99354, USA

⁴ Centre for Climate Change Research, Indian Institute of Tropical Meteorology, Ministry of Earth Sciences, Dr. Homi Bhabha Road, Pune 411008, Maharashtra, India

⁵ NORCE Norwegian Research Centre, Bjerknes Centre for Climate Research, Nygårdsgaten 112, Bergen 5008, Norway

⁶ Department of Meteorology and Atmospheric Science, and Center for Advanced Data Assimilation and Predictability Techniques, The Pennsylvania State University, Walker Building, University Park, PA 16802, USA

⁷ Department of Earth Sciences, University of Gothenburg, Guldhedsgatan 5A, Gothenburg 40530, Sweden

⁸ National Tibetan Plateau Data Center, State Key Laboratory of Tibetan Plateau Earth System and Resource Environment, Institute of Tibetan Plateau Research, Building 3, No.16 Lincui Road, Beijing 100101, China

⁹ Japan Agency for Marine-Earth Science and Technology, 3173-25 Showa-machi, Kanazawa-ku, Yokohama 2360001, Japan

¹⁰ Swedish Meteorological and Hydrological Institute (SMHI), Folkborgsvägen 17, Norrköping 601 76, Sweden

¹¹ Nanjing University (NJU), 163 Xianlin Road, Qixia District, Nanjing 210023, Jiangsu Province, China

¹² Institute of Atmospheric Physics, Chinese Academy of Sciences, HuaYanLi No. 40, QiJiaHuoZi, ChaoYang District, BeiJing 100049, China

¹³ HAREME Lab, Institute of Geography, Center for Earth System Research and Sustainability (CEN), Universität Hamburg, Bundesstrasse 55, Hamburg 20146, Hamburg, Germany

¹⁴ Cardiff University, Park Place, Cardiff, Wales CF10 3AT, UK

¹⁵ University of Bergen, P.O.Box 7800, Bergen 5020, Norway

¹⁶ Institute for Atmospheric and Environmental Sciences, Goethe University, Altenhöferallee 1, Frankfurt am Main 60438, Hesse, Germany

¹⁷ Present Address: Karlsruhe Institute of Technology (KIT), Hermann-von-Helmholtz-Platz 1, Eggenstein-Leopoldshafen 76344, Baden-Württemberg, Germany

¹⁸ Laboratoire des Sciences du Climat et de l'Environnement, IPSL, UMR 8212, CEA-CNRS-UVSQ-UPS, Gif sur Yvette, France

¹⁹ Department of Geophysics, Faculty of Science, University of Zagreb, Horvatovac 95, Zagreb, Croatia

¹ MMM Laboratory, National Center for Atmospheric Research, 3090 Center Green Dr., Boulder 80301, CO, USA